

# 1 **Effective radiative forcing from emissions of reactive gases and** 2 **aerosols – a multi-model comparison**

3 Gillian D. Thornhill<sup>1</sup>, William J. Collins<sup>1</sup>, Ryan J. Kramer<sup>2</sup>, Dirk Olivie<sup>3</sup>, Ragnhild B. Skeie<sup>4</sup>,  
4 Fiona M. O'Connor<sup>5</sup>, Nathan Luke Abraham<sup>6,7</sup>, Ramiro Checa-Garcia<sup>8</sup>, Susanne E. Bauer<sup>9</sup>,  
5 Makoto Deushi<sup>10</sup>, Louisa K. Emmons<sup>11</sup>, Piers M. Forster<sup>12</sup>, Larry W. Horowitz<sup>13</sup>, Ben  
6 Johnson<sup>5</sup>, James Keeble<sup>7</sup>, Jean-Francois Lamarque<sup>11</sup>, Martine Michou<sup>14</sup>, Michael J. Mills<sup>11</sup>,  
7 Jane P. Mulcahy<sup>5</sup>, Gunnar Myhre<sup>4</sup>, Pierre Nabat<sup>14</sup>, Vaishali Naik<sup>13</sup>, Naga Oshima<sup>10</sup>, Michael  
8 Schulz<sup>3</sup>, Christopher J. Smith<sup>12,18</sup>, Toshihiko Takemura<sup>15</sup>, Simone Tilmes<sup>11</sup>, Tongwen Wu<sup>16</sup>,  
9 Guang Zeng<sup>17</sup>, Jie Zhang<sup>16</sup>.

10 <sup>1</sup>Department of Meteorology, University of Reading, Reading, RG6 6BB, UK

11 <sup>2</sup>Climate and Radiation Laboratory, NASA Goddard Space Flight Center, Greenbelt, MD 20771, USA, and  
12 Universities Space Research Association, 7178 Columbia Gateway Drive, Columbia, MD 21046, USA

13 <sup>3</sup>Norwegian Meteorological Institute, Oslo, Norway

14 <sup>4</sup>CICERO – Centre for International Climate and Environmental Research Oslo, Oslo, Norway

15 <sup>5</sup>Met Office, Exeter, UK

16 <sup>6</sup>National Centre for Atmospheric Science, U.K

17 <sup>7</sup>Department of Chemistry, University of Cambridge, Lensfield Road, Cambridge, CB2 1EW, U.K.,

18 <sup>8</sup>Laboratoire des Sciences du Climat et de l'Environnement, IPSL/CNRS, 91191 Gif Sur Yvette, France

19 <sup>9</sup> NASA Goddard Institute for Space Studies, USA

20 <sup>10</sup> Meteorological Research Institute, Tsukuba, Japan

21 <sup>11</sup> National Center for Atmospheric Research, Boulder, CO, USA

22 <sup>12</sup> University of Leeds, Leeds, UK

23 <sup>13</sup> NOAA, Geophysical Fluid Dynamics Laboratory (GFDL), Princeton, NJ 08540-6649

24 <sup>14</sup> CNRM, Université de Toulouse, Météo-France, CNRS, Toulouse, France

25 <sup>15</sup> Research Institute for Applied Mechanics, Kyushu University, Japan

26 <sup>16</sup> Climate System Modeling Division, Beijing Climate Center, Beijing, China

27 <sup>17</sup> National Institute of Water and Atmospheric Research (NIWA), Wellington, New Zealand

28 <sup>18</sup>International Institute for Applied Systems Analysis (IIASA), Laxenburg, Austria

29  
30 *Correspondence to:* Gillian D. Thornhill (g.thornhill@reading.ac.uk)

## 31 **Abstract**

32 This paper quantifies the pre-industrial (1850) to present-day (2014) effective radiative forcing (ERF) of  
33 anthropogenic emissions of NO<sub>x</sub>, VOCs (including CO), SO<sub>2</sub>, NH<sub>3</sub>, black carbon, organic carbon, and  
34 concentrations of methane, N<sub>2</sub>O and ozone-depleting halocarbons, using CMIP6 models. Concentration and

35 emission changes of reactive species can cause multiple changes in the composition of radiatively active species:  
36 tropospheric ozone, stratospheric ozone, stratospheric water vapour, secondary inorganic and organic aerosol and  
37 methane. Where possible we break down the ERFs from each emitted species into the contributions from the  
38 composition changes. The ERFs are calculated for each of the models that participated in the AerChemMIP  
39 experiments as part of the CMIP6 project, where the relevant model output was available.

40 The 1850 to 2014 multi-model mean ERFs ( $\pm$  standard deviations) are  $-1.03 \pm 0.37 \text{ Wm}^{-2}$  for  $\text{SO}_2$  emissions, -  
41  $0.25 \pm 0.09 \text{ Wm}^{-2}$  for organic carbon (OC),  $0.15 \pm 0.17 \text{ Wm}^{-2}$  for black carbon (BC) and for  $\text{NH}_3$  it is  $-0.07 \pm$   
42  $0.01 \text{ Wm}^{-2}$ . For the combined aerosols (in the piClim-aer experiment) it is  $-1.01 \pm 0.25 \text{ Wm}^{-2}$ . The multi-model  
43 means for the reactive well-mixed greenhouse gases (including any effects on ozone and aerosol chemistry) are  
44  $0.67 \pm 0.17 \text{ Wm}^{-2}$  for methane ( $\text{CH}_4$ ),  $0.26 \pm 0.07 \text{ Wm}^{-2}$  for nitrous oxide ( $\text{N}_2\text{O}$ ) and  $0.12 \pm 0.2 \text{ Wm}^{-2}$  for ozone-  
45 depleting halocarbons (HC). Emissions of the ozone precursors nitrogen oxides ( $\text{NO}_x$ ), volatile organic  
46 compounds (VOC) and both together ( $\text{O}_3$ ) lead to ERFs of  $0.14 \pm 0.13 \text{ Wm}^{-2}$ ,  $0.09 \pm 0.14 \text{ Wm}^{-2}$  and  $0.20 \pm 0.07$   
47  $\text{Wm}^{-2}$  respectively. The differences in ERFs calculated for the different models reflect differences in the  
48 complexity of their aerosol and chemistry schemes, especially in the case of methane where tropospheric  
49 chemistry captures increased forcing from ozone production.

50

## 51 **1. Introduction**

52 The characterisation of the responses of the atmosphere, climate, and earth systems to various forcing agents is  
53 essential for understanding, and countering, the impacts of climate change. As part of this effort there have been  
54 several projects directed at using climate models from different groups around the world to produce a systematic  
55 comparison of the simulations from these models, via the Coupled Model Intercomparison Project (CMIP), which  
56 is now in its 6<sup>th</sup> iteration (Eyring et al., 2016). This CMIP work has been subdivided into different areas of interest  
57 for addressing specific questions about climate change, such as the impact of aerosols and reactive greenhouse  
58 gases, and the AerChemMIP (Collins et al., 2017) project is designed to examine the specific effects of these  
59 factors on the climate. The aerosol and aerosol precursor species considered are sulphur dioxide ( $\text{SO}_2$ ), black  
60 carbon (BC), organic carbon (OC). The reactive greenhouse gases and ozone precursors are methane ( $\text{CH}_4$ ),  
61 nitrogen oxide ( $\text{NO}_x$ ), volatile organic compounds (VOCs – including carbon monoxide), nitrous oxide ( $\text{N}_2\text{O}$ )  
62 and ozone-depleting halocarbons (HC).

63 The focus of this work is to characterise the effect of the change from pre-industrial (1850) to present day (2014)  
64 in aerosols and their precursors, and chemically-reactive greenhouse gases (including species that affect ozone)  
65 on the radiation budget of the planet, referred to as radiative forcing, as an initial step to understanding the response  
66 of the atmosphere and earth system to changes in these components. In previous reports of the Intergovernmental  
67 Panel on Climate Change (IPCC) the effect of the various forcing agents on the radiation balance has been  
68 investigated in terms of the radiative forcing, (RF), which is a measure of how the radiative fluxes at the top of  
69 atmosphere (TOA) change in response to changes in, e.g., concentrations or emissions of greenhouse gases and  
70 aerosols. There have been several definitions of radiative forcing, (Forster et al., 2016; Sherwood et al., 2015),  
71 which generally considered the instantaneous radiative forcing (IRF), or a combination of the IRF including the  
72 adjustment of the stratospheric temperature to the driver, generally termed the stratospheric-temperature adjusted  
73 radiative forcing. More recently (Boucher, 2013; Chung and Soden, 2015) there has been a move towards using

74 the effective radiative forcing (ERF) as the preferred metric, as this includes the rapid adjustments of the  
75 atmosphere to the perturbation, e.g. changes in cloud cover or type, water vapour, tropospheric temperature, which  
76 may affect the overall radiative balance of the atmosphere. In this work, ERF is calculated using two atmospheric  
77 model simulations both with the same prescribed sea-surface temperatures (SSTs) and sea ice, but one having the  
78 perturbation we are interested in investigating, e.g. a change in emissions or concentrations of aerosols or reactive  
79 gases. The difference in the net TOA flux between these two simulations is then defined as the ERF for that  
80 perturbation.

81 Previous efforts to understand the radiative forcing due to aerosols and reactive gases in CMIP simulations have  
82 resulted in a wide spread of values from the different climate models, in part due to a lack of suitable model  
83 simulations for extracting the ERF from, e.g., a specific change to an aerosol species. The experiments in the  
84 AerChemMIP project have been designed to address this in part, by defining consistent model set-ups to be used  
85 to calculate the ERFs, although the individual models will still have their own aerosol and chemistry modules,  
86 with varying levels of complexity and different approaches.

87 There are complexities in assessing how a particular forcing agent affects the climate system due to the interactions  
88 between some of the reactive gases; for example methane and ozone are linked in complex ways, and this increases  
89 the problem of understanding the specific contribution of each to the overall ERF when one of them is perturbed.  
90 An attempt to understand some of these interactions is discussed in Section 4.2 below.

91 The experimental set-up and models used are described in Section 2, the methods for calculating the ERFs for the  
92 aerosol and chemistry experiments are described in Section 3, and the results are discussed in section 4. Final  
93 conclusions are drawn in Section 5.

## 94 **2. Experimental Setup**

### 95 **2.1 Models**

96 This analysis is based on models participating in the Coupled Model Intercomparison Project (CMIP6) (Eyring et  
97 al., 2016), which oversees climate modelling efforts from a number of centres with a view to facilitating  
98 comparisons of the model results in a systematic framework. The overall CMIP6 project has a number of sub-  
99 projects, where those with interests in specific aspects of the climate can design and request specific experiments  
100 to be undertaken by the modelling groups. To understand the effects of aerosols and reactive gases on the climate,  
101 a set of experiments was devised under the auspices of AerChemMIP (Collins et al., 2017), described in Section  
102 2.2.

103 The anthropogenic emissions of the aerosols, aerosol precursors and ozone precursors (excluding methane) for  
104 use in the models are given by Hoesly et al. (2018) and van Marle et al. (2017). Models use their own natural  
105 emissions (Eyring et al., 2016). The well-mixed greenhouse gases (WMGHG), CO<sub>2</sub>, CH<sub>4</sub>, N<sub>2</sub>O and halocarbons  
106 are specified as concentrations either at the surface or in the troposphere. Not all of the models include interactive  
107 aerosols, tropospheric chemistry and stratospheric chemistry, which is the ideal for the AerChemMIP experiments,  
108 but those models which do not include all these processes provide results for a subset of the experiments described  
109 in Section 2.2.

110 The models included in this analysis are summarised below, and in Table 1 with an overview of the model set-up,  
111 aerosol scheme and type of chemistry models used included. A more detailed description of each model and the  
112 aerosol and chemistry schemes used in each is available in the supplementary materials, Table S1.

113 The CNRM-ESM2-1 model (Séférian et al., 2019; Michou et al., 2020) includes an interactive tropospheric aerosol  
114 scheme, and an interactive gaseous chemistry scheme only above the level of 560 hPa. The sulfate precursors  
115 evolve to SO<sub>4</sub> using a simple dependence on latitude. The cloud droplet number concentration (CDNC) depends  
116 on SO<sub>4</sub>, organic matter and sea-salt concentrations, so the aerosol cloud-albedo effect is represented, although  
117 other aerosol-cloud interactions are not.

118 The UKESM1 model (Sellar et al., 2020) includes an interactive stratosphere-troposphere gas-phase chemistry  
119 scheme (Archibald et al., 2020) using the UK Chemistry and Aerosol (UKCA); (Morgenstern et al.,  
120 2009; O'Connor et al., 2014) model. The UKCA aerosol scheme, called GLOMAP-mode is two-moment  
121 simulation of tropospheric black carbon, organic carbon, SO<sub>4</sub> and sea salt. Dust is modelled independently using  
122 the bin scheme of Woodward (2001). A full description and evaluation of the chemistry and aerosol schemes in  
123 UKESM1 can be found in Archibald et al. (2020) and Mulcahy et al. (2020) respectively.

124 The MIROC6 model includes the Spectral Radiation-Transport Model for Aerosol Species (SPRINTARS) aerosol  
125 model which predicts mass mixing ratios of the main tropospheric aerosols and models aerosol-cloud interactions  
126 in which aerosols alter cloud microphysical properties and affect the radiation budget by acting as cloud  
127 condensation and ice nuclei (Takemura et al., 2005; Watanabe et al., 2010; Takemura and Suzuki, 2019; Takemura,  
128 2018; Tatebe et al., 2019).

129 The MRI-ESM2 model (Yukimoto et al., 2019) has the Model of Aerosol Species in the Global Atmosphere mark-  
130 2 revision 4-climate (MASINGAR mk-2r4c) aerosol model, and a chemistry model, MRI-CCM2 (Deushi and  
131 Shibata, 2011) which models chemistry processes for ozone and other trace gases from the surface to middle  
132 atmosphere. The model includes aerosol-chemistry interactions, and aerosol-cloud interactions (Kawai et al.,  
133 2019). The ERFs of anthropogenic gases and aerosols under present-day conditions relative to preindustrial  
134 conditions estimated by MRI-ESM2 as part of the Radiative Forcing Model Intercomparison Project (RFMIP)  
135 (Pincus et al., 2016) and AerChemMIP are summarized in Oshima et al. (2020).

136 The BCC-ESM1 model (Wu et al., 2019; Wu et al., 2020) models major aerosol species including gas-phase  
137 chemical reactions, secondary aerosol formation, and aerosol-cloud interactions including indirect effects are  
138 represented. It does not include stratospheric chemistry, so concentrations of ozone, CH<sub>4</sub>, and N<sub>2</sub>O at the top two  
139 model levels are the zonally and monthly values derived from the CMIP6 data package.

140 The NorESM2 model contains interactive aerosols and uses the OsloAero6 aerosol module (Seland et al., 2020),  
141 (Olivie et al., in prep.) describes the formation and evolution of BC, OC, SO<sub>4</sub>, dust, sea-salt and SOA. There is a  
142 limited gas-phase chemistry describing the oxidation of the aerosol precursors DMS, SO<sub>2</sub>, isoprene, and  
143 monoterpenes and oxidant fields of OH, HO<sub>2</sub>, NO<sub>3</sub> and ozone are prescribed climatological fields, and there is no  
144 ozone chemistry in the model.

145 The GFDL-ESM4 model consists of the GFDL AM4.1 atmosphere component, (Dunne et al., 2020; Horowitz et  
146 al., 2020) which includes an interactive tropospheric and stratospheric gas-phase and aerosol chemistry scheme.  
147 Nitrate aerosols are explicitly treated in this model.

148 The CESM2-WACCM model includes interactive chemistry and aerosols for the troposphere, stratosphere and  
149 lower thermosphere (Emmons et al., 2010); (Gettelman et al., 2019). The representation of secondary organic  
150 aerosols follows the Volatility Basis Set approach (Tilmes et al., 2019).

151 The IPSLCM6A-LR-INCA (referred to subsequently as IPSL-INCA) model used for this analysis has interactive  
152 aerosols but a limited gas-phase model. The aerosol scheme is based on a sectional approach with to represent the

153 size distribution of dust, sea- salt (which has an additional super-coarse mode to model largest emission of spray-  
 154 salt aerosols), BC, NH<sub>4</sub>, NO<sub>3</sub>, SO<sub>4</sub>, SO<sub>2</sub> and OA with a combination of accumulation and coarse log-normal modes  
 155 with both soluble and insoluble treated as independent modes. DMS emissions are prescribed and not interactively  
 156 calculated. BC is modelled as internally mixed with sulphate (Wang et al. (2016), where the refractive index is  
 157 relies on Garnet-Maxwell method. Its emissions are derived from inventories. A new dust refractive index is  
 158 implemented (Di Biagio et al., 2019). Well mixed trace gases concentrations/emissions are forced with  
 159 AMIP/CMIP6 datasets (Lurton et al., 2020) ozone using Checa-Garcia et al. (2018) and solar forcing from Matthes  
 160 et al. (2017).

161 The GISS-E2-1 model aerosol scheme (One-Moment Aerosol (OMA)) module, which includes sulfate, nitrate,  
 162 ammonium, carbonaceous aerosols (BC and OC), is coupled to both the tropospheric and stratospheric chemistry  
 163 scheme. For the results reported here, the physics version 3 of this model configuration was used, which includes  
 164 the aerosol impacts on clouds. For details of the model, see Bauer et al. (2020).

165

166 **Table 1 Components used in the Earth system models (detailed Table is in Supplementary material, Table S1)**

	Aerosols	Tropospheric chemistry	Stratospheric chemistry
IPSL-CM6A-LR-INCA	Interactive	No	No
NorESM2-LM	Interactive	SOA and sulfate precursor chemistry	No
UKESM1-LL	Interactive Tropospheric. Prescribed stratospheric	Interactive	Interactive
CNRM-ESM2-1	Interactive	Chemical reactions down to 560 hPa	Interactive
MRI-ESM2	Interactive	Interactive	Interactive
MIROC6	Interactive	SOA and sulfate precursor chemistry	No
BCC-ESM1	Interactive	Interactive	No
GFDL-ESM4	Interactive	Interactive	Interactive
CESM2-WACCM	Interactive	Interactive	Interactive
GISS-E2-1	Interactive	Interactive	Interactive

167 **2.2 Experiments**

168 The AerChemMIP timeslice experiments (Table 2) are used to determine the present-day (2014) ERFs for the  
 169 changes in emissions or concentrations of reactive gases, and aerosols or their precursors (Collins et al., 2017).

170 The ERFs are calculated by comparing the change in net TOA radiation fluxes between two runs with the same

171 prescribed sea surface temperatures (SSTs) and sea ice, but with near-term climate forcers (NTCFs - also referred  
 172 to as short-lived climate forcers - SLCFs), reactive gas and aerosol emissions, and well-mixed greenhouse gases  
 173 (WGMHG - methane, nitrous oxide, halocarbon) concentrations perturbed. It should be noted that in  
 174 AerChemMIP the NTCF experiment excludes CH<sub>4</sub> the experimental design. The control run uses set 1850 pre-  
 175 industrial values for the aerosol and aerosol precursors, CH<sub>4</sub> N<sub>2</sub>O, ozone precursors and halocarbons, either as  
 176 emissions or concentrations (Hoesly et al., 2018;van Marle et al., 2017;Meinshausen et al., 2017). Monthly  
 177 varying prescribed SSTs and sea-ice are taken from the CMIP6 DECK coupled pre-industrial (1850) control  
 178 simulation. Each experiment then perturbs the pre-industrial value by changing one (or more) of the species  
 179 (emissions or concentrations) to the 2014 value, while keeping SSTs and sea-ice prescribed as in the pre-industrial  
 180 control. Note adding individual species to a pre-industrial control will likely give different results to a setup where  
 181 species were individually subtracted from a present-day control. The NTCFs are perturbed individually or in  
 182 groups. This provides ERFs for the specific emission or concentration change, but also for all aerosol precursor  
 183 or NTCFs combined (Collins et al., 2017). For models without interactive tropospheric chemistry “NTCF” and  
 184 “aer” experiments are the same; in the case of NorESM2 for the NTCF experiments the model attempts to mimic  
 185 the full chemistry by setting the oxidants and ozone to 2014 values. The WGMHG experiments include the effects  
 186 on aerosol oxidation, tropospheric and stratospheric ozone, and stratospheric water vapour depending on the  
 187 model complexity.

188 Thirty years of simulation are required to minimise internal variability (mainly from clouds) (Forster et al, 2016.),  
 189 and one ensemble member was used for each experiment (almost all models provided only a single ensemble  
 190 member).

191

192 **Table 2 List of fixed SST ERF simulations. (NTCF in (Collins et al., 2017) is also referred to as 'SLCF' - short-lived**  
 193 **climate forcers - in other publications) and for the purposes of this study excludes methane.**

Experiment ID	CH <sub>4</sub>	N <sub>2</sub> O	Aerosol Precursors	Ozone Precursors	CFC/ HCFC	Number of models
<i>piClim-control</i>	1850	1850	1850	1850	1850	11
<i>piClim-NTCF</i>	1850	1850	<b>2014</b>	<b>2014</b>	1850	8
<i>piClim-aer</i>	1850	1850	<b>2014</b>	1850	1850	9
<i>piClim-BC</i>	1850	1850	1850 (non BC) <b>2014 (BC)</b>	1850	1850	7
<i>piClim-O3</i>	1850	1850	1850	<b>2014</b>	1850	4
<i>piClim-CH4</i>	<b>2014</b>	1850	1850	1850	1850	8
<i>piClim-N2O</i>	1850	<b>2014</b>	1850	1850	1850	5
<i>piClim-HC</i>	1850	1850	1850	1850	<b>2014</b>	6
<i>piClim-NOX</i>	1850	1850	1850	1850 (non NO <sub>x</sub> ) <b>2014 (NO<sub>x</sub>)</b>	1850	5
<i>piClim-VOC</i>	1850	1850	1850	1850 (non CO/VOC) <b>2014 (CO/VOC)</b>	1850	5
<i>piClim-SO2</i>	1850	1850	1850 (non SO <sub>2</sub> ) <b>2014 (SO<sub>2</sub>)</b>	1850	1850	6

<i>piClim-OC</i>	1850	1850	1850 (non OC) <b>2014 (OC)</b>	1850	1850	6
<i>piClim-NH3</i>	1850	1850	1850 (non NH <sub>3</sub> ) <b>2014 (NH<sub>3</sub>)</b>	1850	1850	2

### 194 3. Methods

195 In the following analysis we use several methods to analyse the ERF and the relative contributions from different  
 196 aerosols, chemistry and processes to the overall ERF for the models and experiments described above, where the  
 197 appropriate model diagnostics were available.

#### 198 3.1 Calculation of ERF using fixed SSTs

199 The ERF is calculated from the experiments described above, where the sea surface temperatures and sea-ice are  
 200 fixed to climatological values. Here the ERF is defined as the difference in the net TOA flux between the perturbed  
 201 experiments and the piClim-control experiment (Sherwood et al., 2015), calculated as the global mean for the 30  
 202 years of the experimental run (where the models were run longer than 30 years, only the last 30 years was used).  
 203 This allows us to calculate the ERF for the individual species based on the changes to the emission or  
 204 concentrations between the control and perturbed runs of the models. The assumption is that there is minimal  
 205 contribution from the climate feedback when the SSTs are fixed, but the resultant ERF includes rapid adjustments  
 206 to the forcing agent in the atmosphere (Forster et al., 2016).

207 The ERF calculated using this method includes any contributions to the ERF resulting from changes in the land  
 208 surface temperature ( $T_s$ ), which ideally should be removed (Shine et al., 2003; Hansen et al., 2005; Vial et al., 2013)  
 209 (as the ocean temperature changes are removed by using fixed SSTs). However, there is no simple way to prescribe  
 210 land surface temperatures in the models considered here analogous to the fixing the SSTs, so we make the land  
 211 surface temperature correction by calculating the surface temperature adjustment from the radiative kernel (see  
 212 Section 3.2) and subtracting it from the standard ERF as calculated above (see also Smith et al. (2020a); (Tang et  
 213 al., 2019)). This is designated the ERF<sub>ts</sub> to differentiate it from the standard ERF as described above.

#### 215 3.2 Kernel Analysis

216 Where the relevant data are available, we use the radiative kernel method (Smith et al., 2018; Soden et al.,  
 217 2008; Chung and Soden, 2015) to break down the ERF into the instantaneous radiative forcing (IRF) and individual  
 218 rapid adjustments (designated by A) which are radiative responses to changes in atmospheric state variables that  
 219 are not coupled to surface warming. In this approach, ERF is defined as:

$$220 \text{ ERF} = \text{IRF} + A_{t\_trop} + A_{t\_strat} + A_{ts} + A_q + A_a + A_c + e \quad (1)$$

221 where  $A_{t\_trop}$  is the troposphere temperature adjustment,  $A_{t\_strat}$  is the troposphere temperature adjustment,  $A_{ts}$  is  
 222 the surface temperature adjustment,  $A_q$  is the water vapour adjustment,  $A_a$  is the albedo adjustment,  $A_c$  is the cloud  
 223 adjustment, and  $e$  is the radiative kernel error. Individual rapid adjustments ( $A_x$ ) are computed as:

224

225 
$$A_x = \frac{\delta R}{\delta x} dx \tag{2}$$

226 where  $\frac{\delta R}{\delta x}$  is the radiative kernel, a diagnostic tool typically computed with an offline version of a GCM radiative  
 227 transfer model that is initialized with climatological base state data and  $dx$  is the climate response of atmospheric  
 228 state variable  $x$ , diagnosed directly from each model. Cloud rapid adjustments ( $A_c$ ) are estimated by diagnosing  
 229 cloud radiative forcing from model flux diagnostics and correcting for cloud masking using the kernel-derived  
 230 non-cloud adjustments and IRF, following common practice (e.g. (Soden et al., 2008;Smith et al., 2018)),  
 231 whereby:

232 
$$A_c = (ERF - ERF^{clr}) - (IRF - IRF^{clr}) - \sum_{x=[T,ts,q,a]} (A_x - A_x^{clr}) \tag{3}$$

233 For the calculation of the IRF (for aerosols this is the direct effect) here, the clear-sky IRF ( $IRF^{clr}$ ) is estimated  
 234 as the difference between clear-sky ERF ( $ERF^{clr}$ ) and the sum of kernel-derived clear-sky rapid adjustments  
 235 ( $A_x^{clr}$ ). Since estimates of  $A_c$  are dependent on IRF, the same differencing method cannot be used to estimate IRF  
 236 under all-sky conditions without special diagnostics (in particular the International Satellite Cloud Climatology  
 237 Project diagnostics (ISCCP) diagnostics) not widely available in the AerChemMIP archive. Instead, for the  
 238 calculations presented here all-sky IRF is computed by scaling  $IRF^{clr}$  by a species-specific factor to account for  
 239 cloud masking (Soden et al. 2008).

240 Kernels are available from several sources, and for this analysis we used kernels from CESM, (Pendergrass et al.,  
 241 2018), GFDL (Soden et al., 2008), HadGEM3, (Smith et al., 2020b), and ECHAM6 (Block and Mauritsen, 2013)  
 242 and took the mean from the four kernels for each model. Overall the individual kernels produced very similar  
 243 results for each model, as reported in Smith et al. (2018).

### 244 **3.3 Calculation of ERF using aerosol-free radiative fluxes**

245 To understand the contributions of various processes to the overall ERF we can attempt to separate the ERF that  
 246 is due to direct radiative forcing from that due to the effects of clouds. Greenhouse gases and aerosols can alter  
 247 the thermal structure of the atmosphere and hence cloud thermodynamics (the semi-direct effect, (Ackerman et  
 248 al., 2000)), and aerosols can act via microphysical effects (e.g. increasing the number of condensation nuclei and  
 249 decreasing the effective radii of cloud droplets, referred to as the aerosol cloud albedo effect and the cloud lifetime  
 250 effect (Twomey, 1974;Albrecht, 1989;Pincus and Baker, 1994). Following the method of Ghan (2013) the  
 251 contribution of the aerosol-radiation interactions to the ERF can be distinguished from that of the aerosol-cloud  
 252 interactions by using a ‘double-call’ method. This means that the model radiative flux diagnostics are calculated  
 253 a second time but ignoring the scattering and absorption by the aerosol – referred to in the equations below with  
 254 the subscript ‘af’. The other effects of the aerosol on the atmosphere (i.e. cloud changes, stability changes,  
 255 dynamics changes) will still be present, however. The IRF<sub>af</sub> as defined here is the direct radiative forcing from  
 256 the aerosol, due to scattering and absorption of radiation. The cloud radiative forcing (ERF<sub>af</sub>) due to the aerosol-  
 257 cloud interactions is then obtained by using the difference between the aerosol-free all-sky fluxes and the aerosol-  
 258 free clear-sky fluxes, which isolates the cloud effects (see Eqns. 4-6, where Eqn. (6) is included for completeness).  
 259 The ERF<sub>af</sub> may include non-cloud rapid adjustments in cloudy regions of the atmosphere. The final term is the  
 260 ERF as calculated from fluxes with neither clouds nor aerosols (ERF<sub>cs,af</sub>).

261 The ERFs are calculated in the same way as for the all-sky ERF described in Section 3.1, except that the all-sky  
 262 radiative flux diagnostics are replaced by the relevant aerosol-free fluxes for both the clear-sky and all-sky cases.



263

264  $IRF_{ari} = (ERF - ERF_{af})$  (4)

265  $ERF_{afi} = ERF_{af} - ERF_{cs,af}$  (5)

266  $ERF_{cs,af} = ERF_{cs,af}$  (6)

267 Separating the IRF in Eqn. (1) into aerosols and greenhouse gas contributions,  $IRF = IRF_{aer} + IRF_{GHG}$ , we can re-  
 268 write Eqns. 4-6.

269  $IRF_{ari} = IRF_{aer}$  (7)

270  $ERF_{afi} = A_C + \sum_{x=[T,ts,q,a]} (A_x - A_x^{clr}) + (IRF_{GHG} - IRF_{GHG}^{clr})$  (8)

271  $ERF_{cs,af} = \sum_{x=[T,ts,q,a]} A_x^{clr} + IRF_{GHG}^{clr}$  (9)

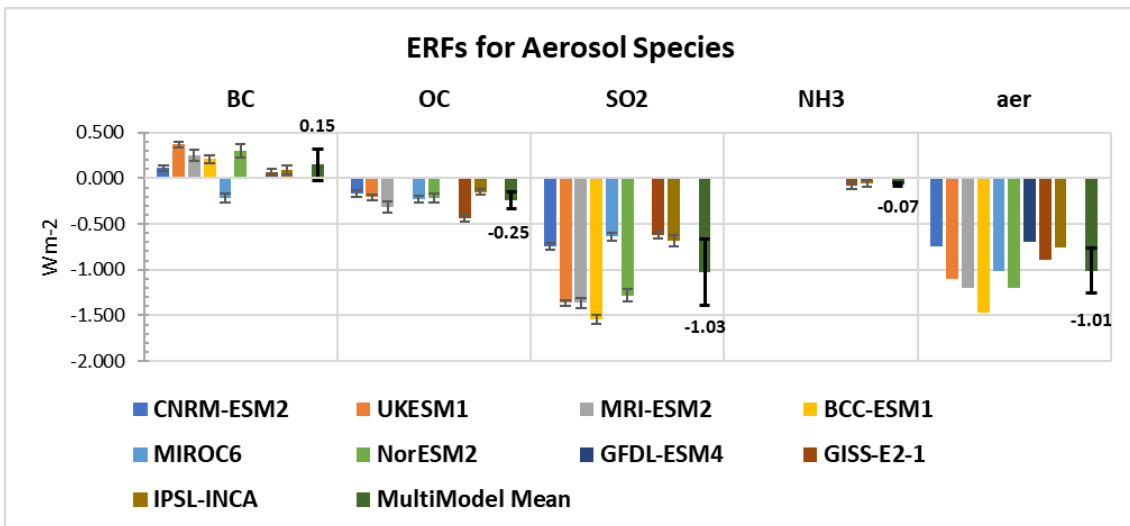
272 So  $ERF_{afi}$  is equivalent to  $A_C$  in Eqn. (3) with extra terms to account for the all-sky - clear-sky difference in the  
 273 non-cloud adjustments and all-sky - clear-sky difference in any greenhouse gas IRF. With no greenhouse gas  
 274 changes  $ERF_{cs,af}$  is the total clear-sky non-cloud adjustment. Ghan (2013) attributes this mostly to the surface  
 275 albedo change  $A_{\alpha}^{clr}$ , however the kernel analysis shows other non-cloud adjustments are larger (Table S4). For  
 276 greenhouse gases  $ERF_{cs,af}$  is the total clear-sky ERF. Assuming the non-cloud adjustments are small apart from  
 277  $T_{strat}$  (Table S4),  $ERF_{cs,af}$  is approximately  $SARF_{GHG}^{clr}$ . The  $SARF_{GHG}^{clr}$  is expected to be an overestimate of  
 278  $SARF_{GHG}$  by 10-40% due to cloud masking (Myhre and Stordal 1997). Thus for greenhouse gases the  $ERF_{afi}$  will  
 279 be a combination of the cloud adjustment and cloud-masking.

280 **4. Results**

281 **4.1 Aerosols and precursors**

282 **4.1.1 Inter-model Variability**

283 The ERFs are calculated as described in Section 3.1, and the summary chart of the ERFs is shown in Fig. 1 for  
 284 those models with available results – it should be noted that not all models ran all the experiments. The multimodel  
 285 mean is shown as a separate bar in Fig. 1, with the value given and the standard error indicated with error bars. A  
 286 table of the individual values for each model and the multimodel mean are included Table S2 in the supplementary  
 287 materials.



288 **Fig. 1 Aerosol ERFs for the models with the available diagnostics for the aerosol species experiments, with interannual**  
289 **variability represented by error bars showing the standard error. The piClim-aer experiments include the BC, OC**  
290 **SO<sub>2</sub> aerosols, and for GISS-E2-1 and IPSL-INCA NH<sub>3</sub> aerosols are also included. The multimodel mean is shown with**  
291 **the mean value and error bars indicating the standard deviation.**

292 For the piClim-BC results, the range of values is from  $-0.21 \text{ Wm}^{-2}$  to  $0.37 \text{ Wm}^{-2}$ , while the MIROC6 model has a  
293 negative ERF for BC, contrasting with the positive values from the other models - see further discussion on this  
294 in Section 4.1.2.

295 The experiments for the OC (organic carbon) have a range from  $-0.44 \text{ Wm}^{-2}$  to  $-0.15 \text{ Wm}^{-2}$ , and the variability  
296 between the models is much less than for the other experiments. The calculated ERFs for the SO<sub>2</sub> experiment  
297 show a variation from  $-1.54 \text{ Wm}^{-2}$  to  $-0.62 \text{ Wm}^{-2}$ , with CNRM-ESM2-1, MIROC6, IPSL-INCA and GISS-E2-1  
298 at the lower end of the range. These models show a smaller rapid adjustment to clouds which would account for  
299 this (see fig S1); also note that CNRM-ESM2-1 does not include aerosol effects apart from the cloud-albedo  
300 effect. The two models with results for the NH<sub>3</sub> (GISS-E2-1 and IPSL-INCA) experiment have ERFs of  $-0.08$  and  
301  $-0.06 \text{ Wm}^{-2}$  respectively.

302 The piClim-aer experiment which uses the 2014 values of aerosol precursors and PI (pre-industrial) values for  
303 CH<sub>4</sub>, N<sub>2</sub>O and ozone precursors shows a range from  $-1.47 \text{ Wm}^{-2}$  to  $-0.7 \text{ Wm}^{-2}$  among the models, making it  
304 difficult to narrow the range of uncertainty of aerosols from global models. However, the range in the CMIP6  
305 models is consistent with that reported in Bellouin et al. (2019), who suggest a probable range of  $-1.60$  to  $-0.65$   
306  $\text{Wm}^{-2}$  for the total aerosol ERF, and compares well with the range of  $-1.37$  to  $-0.63 \text{ Wm}^{-2}$  for the set of piClim-  
307 aer experiments considered in (Smith et al., 2020a) as part of the RFMIP project. In general, the sum of the ERFs  
308 from the individual BC, OC and SO<sub>2</sub> experiments does not equal the piClim-aer experiment, due to non-linearity  
309 in the aerosol-cloud interactions, particularly since the aerosol perturbation is added to the relatively pristine pre-  
310 industrial atmosphere. In the case of GISS and IPSL-INCA, and GFDL-ESM4 the models also include nitrate  
311 aerosols.

312 The issue of the effect of perturbing the pre-industrial atmosphere with the aerosol changes is examined in more  
313 detail in the Supplementary material (see section S6) for NorESM2, where a sensitivity analysis was carried out.  
314 This analysis does not repeat the AerChemMIP experiments with the perturbation in a present-day atmosphere  
315 but examines the effect of adding the SO<sub>2</sub> and combined aerosol perturbation to an already polluted present day  
316 atmosphere. In this simplified sensitivity study the differences are 13% for the SO<sub>2</sub> experiment, and 20% for the  
317 combined aerosol experiment. However, it should be borne in mind that this is for a specific model, and the  
318 perturbed experiment still has the 1850 climate conditions.

319 The ERF<sub>ts</sub> is a simplified method for corrections of land surface warming in fixed sea surface temperature  
320 simulations which in addition to land surface changes leads to changes in land surface albedo changes,  
321 tropospheric temperature, water vapor and cloud changes (Smith et al., 2020a; Tang et al., 2019).

322 The ERF<sub>ts</sub> for the models where the land surface temperature adjustment is removed are also included in  
323 Supplemental Tables S2 and S3, for comparison with the standard ERF. In general, the difference between the  
324 two values is small, of the order of 5 -10%.

325

326 **4.1.2 Breakdown of the ERF into atmospheric adjustments and IRF**

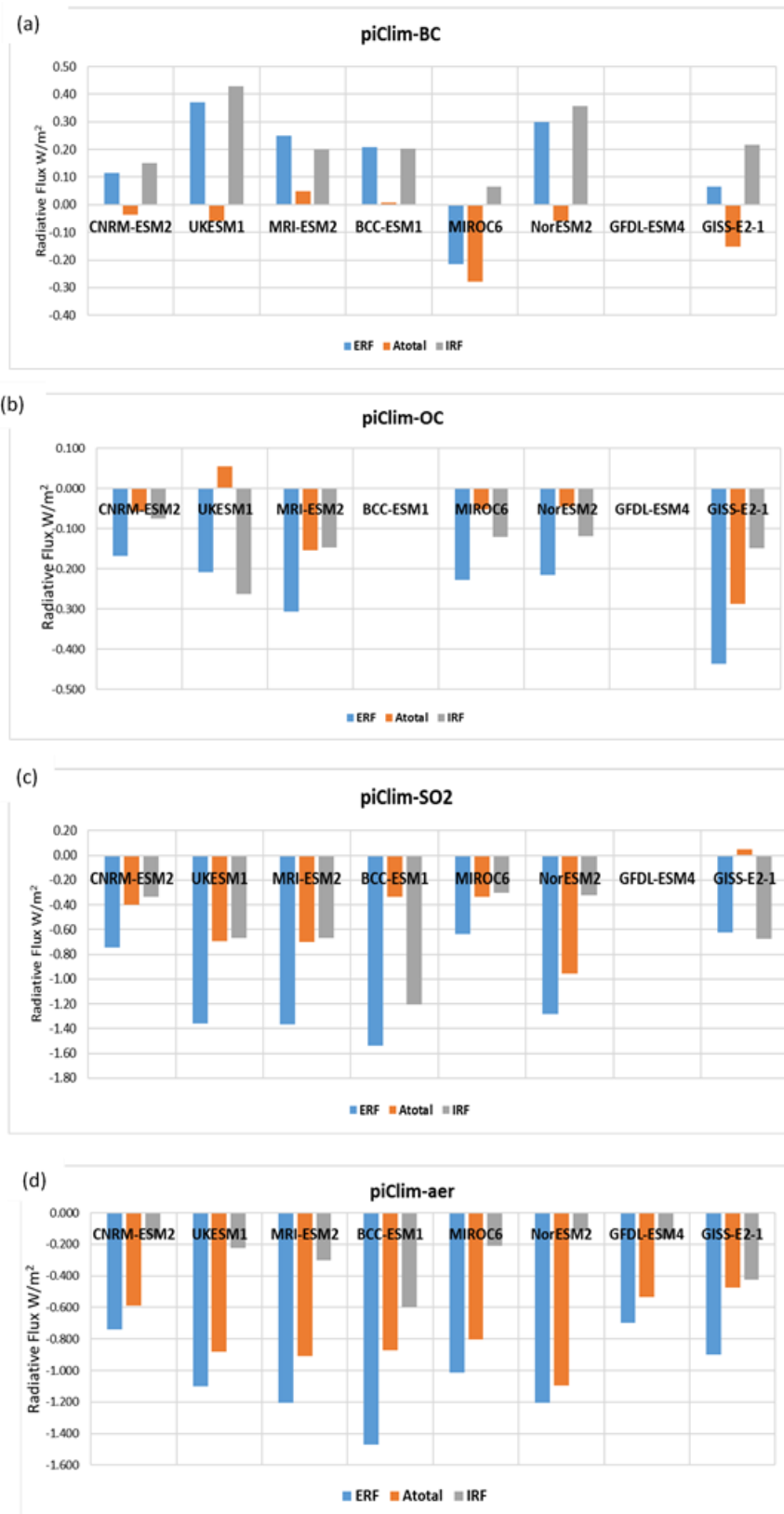


**Figure 2** Breakdown of the ERFs into the atmospheric rapid adjustments (Atotal) and IRF (instantaneous radiative forcing) for the aerosols. (a) piClim-BC experiment, (b) piClim-SO2 experiment, (c) piClim-OC experiment, (d) piClim-aer experiment

328 The results in Fig. 2 show the ERF as calculated from the radiative fluxes in the fixed SST experiments (Section  
 329 3.1), the total of the atmospheric adjustments,  $A_{\text{total}}$ , described in Section 3.2 (where  $A_{\text{total}} = A_T + A_{\text{ts}} + A_q + A_a +$   
 330  $A_c$  c.f. eqn. 1), and the instantaneous radiative forcing (IRF).  
 331 The sum of the IRF and the atmospheric adjustments should equal the overall ERF, however as the calculation of  
 332 the IRF depends upon an empirical factor for cloud masking to find the all-sky IRF from the clear-sky IRF (see  
 333 Section 3.2) the sum of the IRF and the  $A_{\text{total}}$  will not necessarily equal the ERF as calculated directly from the  
 334 model radiative flux diagnostics. However, in general the difference is less than 3%, suggesting that the  
 335 approximation used in the calculation of the IRF is reasonable. Using the kernel method described above it is  
 336 important to note that the IRF calculated here accounts for the presence of the clouds but does not include cloud  
 337 changes such as the cloud albedo effect.  
 338 The models show a variability in the IRF for  $\text{SO}_2$ , (Fig. 2c) with a range of  $-0.3 \text{ Wm}^{-2}$  to  $-1.2 \text{ Wm}^{-2}$  with the BCC-  
 339 ESM1 model being the outlier, having the largest overall ERF. The OC experiments (Fig. 2b) range from  $-0.08$   
 340  $\text{Wm}^{-2}$  to  $-0.26 \text{ Wm}^{-2}$ , with a range for BC of  $0.07 \text{ Wm}^{-2}$  to  $0.43 \text{ Wm}^{-2}$  (Fig. 2a). In MIROC6 the treatment of BC  
 341 (Takemura & Suzuki 2019; Suzuki & Takemura 2019) leads to faster wet removal of BC and hence a lower IRF.  
 342 For the combined aerosols (Fig 2d) the range is from  $-0.1 \text{ Wm}^{-2}$  to  $-0.6 \text{ Wm}^{-2}$ .  
 343 There are significant differences between the models in the  $A_{\text{total}}$  for  $\text{SO}_2$ ; these range from  $0.05 \text{ Wm}^{-2}$  to  $-1.0 \text{ Wm}^{-2}$   
 344  $^2$ , where the differences are dominated by the cloud adjustments which here include the cloud albedo effect as part  
 345 of the adjustment (see Fig S3 for breakdowns of the atmospheric adjustments for all models). The adjustments to  
 346 BC are vary in sign and magnitude, with the MRI-ESM2 and BCC-ESM1 models having a slight positive  
 347 adjustment. The overall model mean has a weaker negative adjustment to that reported by (Stjern et al.,  
 348 2017; Samset et al., 2016; Smith et al., 2018). The MIROC6 model has a large negative adjustment which is large

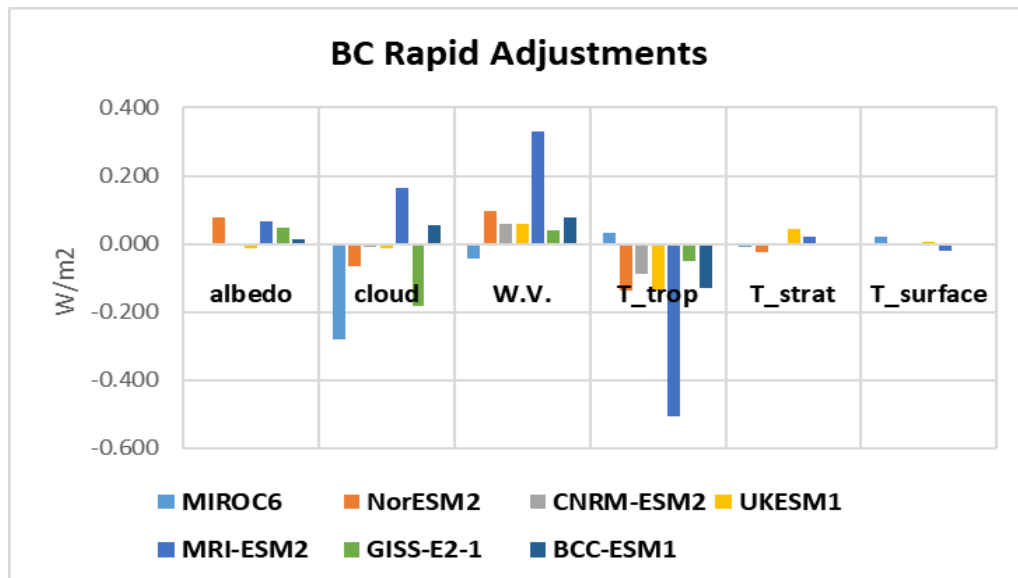


Figure 3 Breakdown of the atmospheric adjustments (albedo, cloud, water vapour, troposphere temperature, stratosphere temperature and surface temperature) for the piClim-BC experiments, showing the variability between models.

349 enough to lead to an overall negative ERF. We explore the contribution of the individual adjustments to BC in  
350 more detail in Fig. 3.

351 Examining the breakdown of the rapid adjustments for the piClim-BC experiments (Fig. 3) we see considerable  
352 variability in the relative importance of the rapid adjustments; the cloud adjustment dominates in MIROC6,  
353 consistent with the increase in low clouds reported for this model, and the treatment of BC as ice nuclei causes  
354 the large negative cloud adjustment here (Takemura and Suzuki, 2019; Suzuki and Takemura, 2019). The GISS-  
355 E2-1 model also has a strong cloud rapid adjustment, but the larger positive value of the IRF leads to an overall  
356 positive ERF for this model. With the exception of MIROC6 the negative tropospheric temperature adjustment is  
357 balanced by the water vapour (specific humidity) adjustment, although the magnitude of these adjustments for  
358 MRI-ESM2 is at least twice that for the other two models. The interaction of BC with clouds in the MRI-ESM2  
359 model is discussed in detail in Oshima et al. (2020), in particular the impact of BC on ice nucleation in high  
360 clouds. The larger surface albedo adjustment for both NorESM2 and MRI-ESM2 is most likely due to the  
361 representation of deposition of BC on snow and ice in these models (Oshima et al., 2020).

362 The piClim-aer experiments (Fig. 1d) show all models have a negative  $A_{\text{total}}$ , covering a range from -0.47 to -1.1  
363  $\text{Wm}^{-2}$ . Overall, the cloud rapid adjustments dominate for the piClim-aer experiments, with a contribution ranging  
364 from -0.45 to -1.1  $\text{Wm}^{-2}$  (See fig S1). Smith et al. (2020) also recently diagnosed forcing and adjustments in a  
365 similar subset of CMIP6 models for the piClim-aer experiment as part of the Radiative Forcing Model  
366 Intercomparison Project (RFMIP) efforts. While they also diagnosed IRF as a residual calculation between ERF  
367 and the sum of rapid adjustments, they estimated cloud adjustments using a modified version of the APRP method  
368 instead of radiative kernels. In their approach, the cloud albedo effect (i.e. Twomey Effect) is considered part of  
369 the IRF, whereas in the traditional kernel decomposition, it is considered a cloud adjustment. Table S5 compares  
370 the two sets of estimates, highlighting the IRF and total cloud adjustment exhibit a near equal absolute difference  
371 between the two studies and the sum of IRF and total cloud adjustment are in close agreement (Mean % difference  
372  $\sim 1.0\%$  for this subset of models). This indicates the classification of the first indirect effect is the only noticeable  
373 difference between the two approaches.

374 The breakdown of the rapid adjustments for all the models are included in supplementary Figure S1, showing the  
375 contributions from each type of rapid adjustment for all the experiments for which we have the relevant  
376 diagnostics.

377

### 378 **4.1.3 Radiation and Cloud interactions**

379 The second method of breaking down the ERF to constituents is described in Section 3.3, (the Ghan method), the  
380 results from which are shown in Table 3. The detailed ERF results for MRI-ESM2 are summarized in Oshima et  
381 al. (2020), and for UKESM1 in O'Connor et al. (2020a). Only four of the models under consideration have so far  
382 produced the necessary diagnostics for this calculation, and the results are presented in Table 3. For the  
383 experiments on aerosols (aer, BC,  $\text{SO}_2$ , OC) the  $\text{ERF}_{\text{cs,af}}$  (non-cloud adjustments) contribution is small, and the  
384 ERF is largely a combination of the direct radiative effect  $\text{IRF}_{\text{ari}}$ , and the cloud radiative effect,  $\text{ERF}_{\text{aci}}$ . The  
385  $\text{IRF}_{\text{ari}}$  is the direct effect of the aerosol due to scattering and absorption, while the  $\text{ERF}_{\text{aci}}$  is the contribution  
386 from the aerosol-cloud interactions and is approximately equal to the rapid adjustments due to clouds ( $A_{\text{c}}$  see  
387 Section 3.2).

388  
389  
390  
391

**Table 3 Results for IRFari, ERFaci and ERFcs,af for aerosol experiments from several models**

	UKESM1			CNRM-ESM2			NorESM2			MRI-ESM2		
	IRFari	ERFcs,af	ERFaci	IRFari	ERFcs,af	ERFaci	IRFari	ERFcs,af	ERFaci	IRFari	ERFcs,af	ERFaci
aer	-0.15	0.05	-1.00	-0.21	0.08	-0.61	0.03	-0.03	-1.21	-0.32	0.09	-0.98
BC	0.37	0.001	-0.005	0.13	0.01	-0.03	0.35	0.07	-0.12	0.26	0.08	-0.09
OC	-0.15	-0.01	-0.07	-0.07	0.04	-0.14	-0.07	0.02	-0.16	-0.07	-0.05	-0.21
SO2	-0.49	0.03	-0.91	-0.29	0.08	-0.53	-0.19	-0.09	-1.01	-0.48	0.05	-0.93

392

393 For the BC experiment the contribution of the aerosol-cloud interaction has a strong contribution to the overall  
394 ERF, except in the case of UKESM1 where it is much weaker; this may be due to the strong SW and LW cloud  
395 adjustments in this model cancelling out (O'Connor et al., 2020; Johnson et al., 2019). The SO<sub>2</sub> experiment shows  
396 a large cloud radiative effect, in fact the ERFaci is mostly double the IRFari in all the models, due to the large  
397 effect on clouds of SO<sub>2</sub> and sulfates through the indirect effects. For the OC experiments the ERFaci to IRFari  
398 comparison is mixed, with the ERFaci general half or less the IRFari, except in the case of UKESM1, where this  
399 ratio is reversed.

400 The IRFari are compared with the IRF calculated via the kernel analysis (Section 3.2) where the relevant model  
401 results are available. These are shown in fig S2(a), the agreement is generally good giving confidence in the kernel  
402 analysis. Similarly ERFaci compares well with the cloud adjustment Ac (fig S2(b)).

403

#### 404 **4.1.4 AOD Forcing Efficiencies**

405 In order to break down the contributions of the constituent aerosol species to the overall aerosol ERF, we use the  
406 AOD (aerosol optical depth) as a forcing efficiency metric for each of the species, and use this to assess their  
407 contributions to the overall ERF. Not all models had diagnostics available for the AOD for the individual species,  
408 so the analysis uses a subset of the models.

409 By looking at the single species piClim-BC, piClim-OC and piClim-SO<sub>2</sub> experiments we can find the change in  
410 the AOD for the individual species (e.g. ΔAOD for BC for the piClim-BC experiment), and use this to scale the  
411 piClim-BC ERF by the AOD change. This assumes that the ERF in the single-species experiment is wholly due  
412 to the change in that species as indicated by the AOD, an assumption which is explored in the Supplementary  
413 material in Section S4. Table 5 shows the AOD forcing efficiency for the piClim-BC, piClim-SO<sub>2</sub> and piClim-  
414 OC experiments for each of the five models which had the relevant optical depth diagnostics available.

415

416 **Table 4 Values of ERF,  $\Delta$ AOD and ERF/AOD for aerosol experiments for CNRM-ESM2-, MIROC6, Nor-ESM2, GISS-**  
 417 **E2-1 and MRI-ESM2 models.**

<b>BC Exp</b>	<b>BC ERF</b>	<b>Change in BC AOD</b>	<b>ERF/AOD</b>
<b>CNRM-ESM2</b>	0.114	0.0015	77.64
<b>MIROC6</b>	-0.214	0.0006	-339.38
<b>NorESM2</b>	0.300	0.0019	159.75
<b>GISS-E2-1</b>	0.065	0.002	31.65
<b>MRI-ESM2</b>	0.251	0.0073	34.22
<b>OC Exp</b>	<b>OC ERF</b>	<b>Change in OA AOD</b>	<b>ERF/AOD</b>
<b>CNRM-ESM2</b>	-0.169	0.0030	-57.20
<b>MIROC6</b>	-0.227	0.0065	-35.05
<b>NorESM2</b>	-0.215	0.0053	-40.57
<b>GISS-E2-1</b>	-0.438	0.0041	-107.16
<b>MRI-ESM2</b>	-0.317	0.0034	-94.39
<b>SO2 Exp</b>	<b>SO2 ERF</b>	<b>Change in SO4 AOD</b>	<b>ERF/AOD</b>
<b>CNRM-ESM2</b>	-0.746	0.0118	-63.22
<b>MIROC6</b>	-0.637	0.0152	-41.91
<b>NorESM2</b>	-1.281	0.0099	-129.24
<b>GISS-E2-1</b>	-0.622	0.0308	-20.22
<b>MRI-ESM2</b>	-1.365	0.0279	-49.08

418 The MIROC6 model results in a negative scaling for BC due to the negative ERF for this experiment for this  
 419 model (Takemura & Suzuki 2019; Suzuki & Takemura 2019) (see Section 4.1.1). The change in the BC AOD is  
 420 similar for CNRM-ESM2-1 and Nor-ESM2, and the scale factors reflect the differences in the ERF. The scaling  
 421 for the SO4 in the NorESM2 experiment is twice that of the other models, suggesting a larger impact of the SO4  
 422 AOD on the ERF in this model. These values differ somewhat from those found in Myhre et al. (2013b) where  
 423 they examined the radiative forcing normalised to the AOD using models in the AeroCom Phase II experiments.  
 424 They found values for sulfate ranging from  $-8 \text{ Wm}^{-2}$  to  $-21 \text{ Wm}^{-2}$  per unit AOD, much weaker than those in our  
 425 results. However, it is important to note that in the AeroCom Phase II experiments the cloud and cloud optical  
 426 properties are identical between their control and perturbed runs, so no aerosol indirect effects are included, nor

427 is any rapid adjustments (IRFari in Eqn. 4). For the BC experiment their values range from  $84 \text{ Wm}^{-2}$  to  $216 \text{ Wm}^{-2}$   
 428  $^2$  per unit AOD, broadly similar to the results presented here (with the exception of the negative MIROC6 result).  
 429 Their results for OA (organic aerosols) which include fossil fuel and biofuel emissions have values ranging from  
 430  $-10 \text{ Wm}^{-2}$  to  $-26 \text{ Wm}^{-2}$  per unit AOD, weaker than our values for the piClim-OC experiments which range from -  
 431  $35 \text{ Wm}^{-2}$  to  $-107 \text{ Wm}^{-2}$  per unit AOD but include the cloud indirect effects here.

432 The sum of the individual AODs from BC,  $\text{SO}_4$ , OA, dust and sea salt gives the total aerosol AOD in the piClim-  
 433 aer experiment, where the various aerosols were combined. We can then use the AOD for each aerosol in the  
 434 piClim-aer experiment and the forcing efficiency above to find the contribution of the individual aerosol to the  
 435 overall change in ERF, providing an approximate estimate of the relative contribution of each aerosol to the overall  
 436 ERF. In Fig. 4 the relative contributions to the ERF from black carbon (BC), organic aerosols (OA) and sulfate  
 437 ( $\text{SO}_4$ ) are shown for three of the models. The sum of the ERFs from the individual species is also compared to the  
 438 ERF calculated from the piClim-aer experiment (NB the sea salt and dust contributions to the ERF are less than

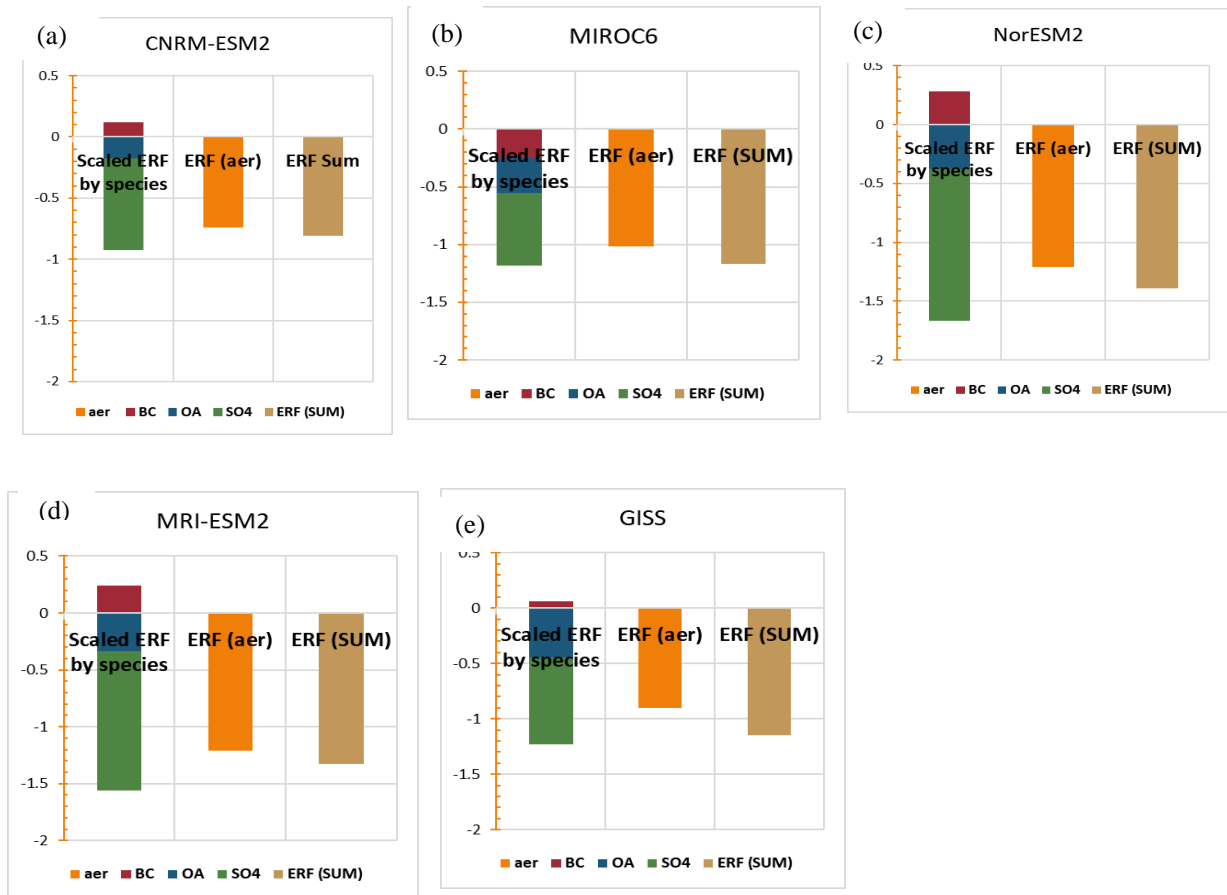


**Fig. 4** The contributions to the ERF for piClim-aer from the individual species, the sum of the scaled ERFs and the ERF calculated directly from the piClim-aer experiment for five of the models.

439 1%, and not shown in this figure for clarity - the ERF/AOD forcing efficiency for these is presented in (Thornhill  
 440 et al., 2020). There is considerable variation in the ERF for the piClim-aer experiments between models (see  
 441 Section 4.1), but from this analysis the  $\text{SO}_4$  is the largest contributor in all cases, although in the case of the  
 442 MIROC6 model its relative importance is reduced. The positive ERF contribution from the BC tends to partly



443 offset the negative ERF from the OA and SO<sub>4</sub>, except in the MIROC6 model, where the BC has a negative  
444 contribution to the ERF.

445 The difference between the calculated ERF from the sum of the scaled ERFs is a result of the non-linearity of the  
446 aerosol-cloud interactions, a factor which is increased because the aerosols are added to the pre-industrial  
447 atmosphere. However, using the IRFari instead of the total ERF to calculate the forcing efficiency and using the  
448 same method also results in a difference between the total IRFari derived from the scaled individual experiments  
449 and the IRFari for the combined aerosol experiment, suggesting that the difference is not simply a result of the  
450 aerosol-cloud interactions.

451 Using the burden as a scaling factor following the same analysis as described for the AOD results in a largely  
452 similar result for the scaling factor, although interestingly the burden scaling for SO<sub>2</sub> in the Nor-ESM2 model is  
453 similar to the other models (see Table S6 for the burden forcing efficiency).

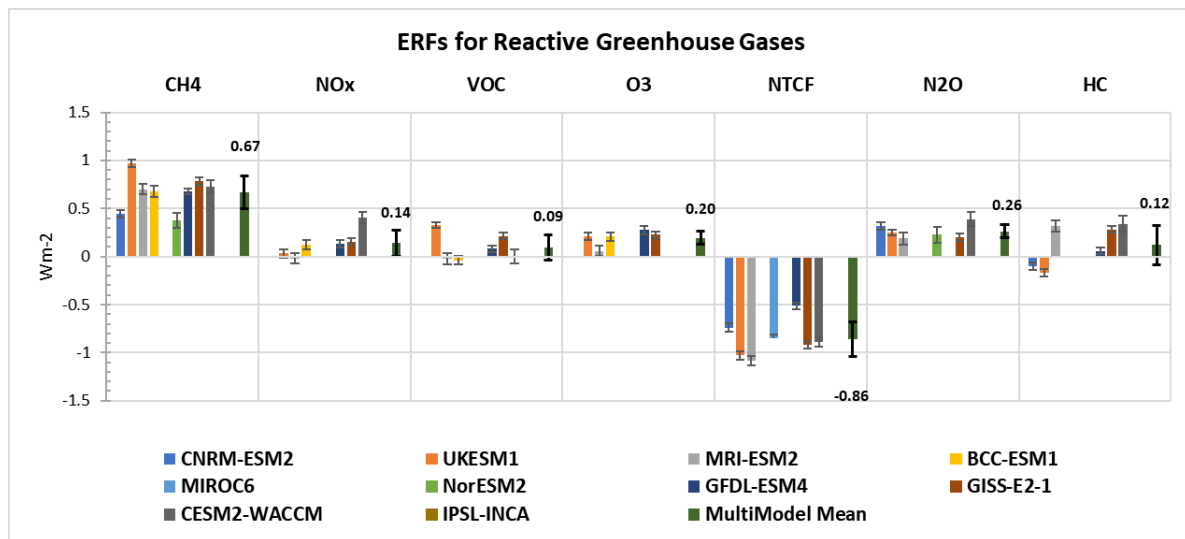
454

## 455 **4.2 Reactive greenhouse gases**

456 The different Earth system models include different degrees of complexity in their chemistry, so their responses  
457 to changes in reactive gas concentrations or emissions differ. NorESM2 has no atmospheric chemistry, so there is  
458 no change to ozone (tropospheric or stratosphere) or to aerosol oxidation following changes in methane or N<sub>2</sub>O  
459 concentrations. CNRM-ESM2-1 includes stratospheric ozone chemistry, but no non-methane hydrocarbon  
460 chemistry and so ozone is prescribed below 560 hPa. There are no effects of chemistry on aerosol oxidation. BCC-  
461 ESM1 includes tropospheric chemistry, but not stratospheric chemistry. Stratospheric concentrations are relaxed  
462 towards climatological values. UKESM1, GFDL-ESM4, CESM2-WACCM, GISS-E2 and MRI-ESM2 all include  
463 tropospheric and stratospheric ozone chemistry as well as changes to aerosol oxidation rates. The ERFs calculated  
464 for the reactive gases for several models are shown in Fig. 5, with the multi-model means given in Supplementary  
465 Table S3.

466 The contributions from gas-phase and aerosol changes to the ERF can be pulled apart to some extent by using the  
467 clear-sky and aerosol-free radiation diagnostics (Table 5). The direct aerosol forcing (IRFari) is diagnosed as for  
468 the aerosol experiments (section 3.3). The diagnosed changes in aerosol mass are shown in Table S8. GFDL-  
469 ESM4 and GISS-ES-1 include nitrate aerosol and show expected responses from NO<sub>x</sub> emissions (including O<sub>3</sub>  
470 experiment). CESM2-WACCM shows an increase in secondary organic aerosol from VOC emissions. Sulphate  
471 responses are generally inconsistent across the models. There seems little correlation between aerosol mass  
472 changes and diagnosed IRFari.

473 For gas-phase experiments the diagnosed cloud interactions (ERFaf-ERFcs,af) comprise the ERFaci from effects  
474 on aerosol chemistry (as in section 3.3) but also any cloud adjustments and effects of cloud masking on the gas-  
475 phase forcing (Eqn. 8). The clear-sky aerosol-free diagnostic (ERFcs,af) is an indication of the greenhouse gas  
476 forcing however this will be an over-estimate as it neglects cloud masking effects (section 3.3).



478 **Fig. 5** Reactive gas ERFs for the models with the available diagnostics for the reactive gas experiments with interannual  
 479 variability represented by error bars showing the standard error. The multimodel mean is shown with the mean value  
 480 and error bars indicating the standard deviation.

#### 481 4.2.1 ERF vs SARF

482 For the reactive greenhouse gases the kernel analysis is used to break down the ERF into the stratospherically  
 483 adjusted radiative forcing (SARF), which is calculated using the IRF from the kernel analysis (Section 3.2) and  
 484 the stratospheric temperature adjustment ( $A_{t\_strat}$ ) ( $SARF = IRF + A_{t\_strat}$ ), and the tropospheric adjustments,  $A_{t\_trop}$ ,  
 485 which is the sum of the tropospheric atmospheric adjustments. These quantities are plotted in Fig. 6.

486 For methane the ERFs are largest for those models that include tropospheric ozone chemistry reflecting the  
 487 increased forcing from ozone production, see section 4.2.2. The analytic calculation for  $CH_4$ -only based on  
 488 Etminan et al. (2016) gives a SARF of  $0.56 \text{ Wm}^{-2}$ . The tropospheric adjustments are negative for all models except  
 489 UKESM1 (Fig 6). The negative cloud adjustment comes from an increase in the LW emissions, possibly due to  
 490 less high cloud. In UKESM1 (O'Connor et al., 2020b) show that methane decreases sulfate new particle  
 491 formation, thus reducing cloud albedo and hence a positive cloud adjustment in that model.

492 For  $N_2O$  results are available for models CNRM-ESM2, NorESM2, MRI-ESM2, and GISS-E2 (the analytic  $N_2O$ -  
 493 only calculation gives a SARF of  $0.17 \text{ Wm}^{-2}$ ). There appears little net rapid adjustment to  $N_2O$  apart from CESM2-  
 494 WACCM. Note that due to the method of calculating the all-sky IRF (section 3.2), the IRF and the adjustment  
 495 terms do not sum to give the ERF.

496 The models respond very differently to changes in halocarbons. The expected halocarbon-only SARF is  $+0.30$   
 497  $\text{Wm}^{-2}$  depending on exact speciation used in the model (WMO 2018). For CNRM-ESM2, UKESM1 and GFDL-  
 498 ESM4 the ERFs are negative or only slightly positive (see also Morgenstern et al. (2020)), whereas for GISS-E2-1  
 499 and MRI-ESM2 the ERFs and SARF are both strongly positive. The differences in stratospheric ozone destruction  
 500 in these models can partially explain the inter-model differences (section 4.2.2).

501

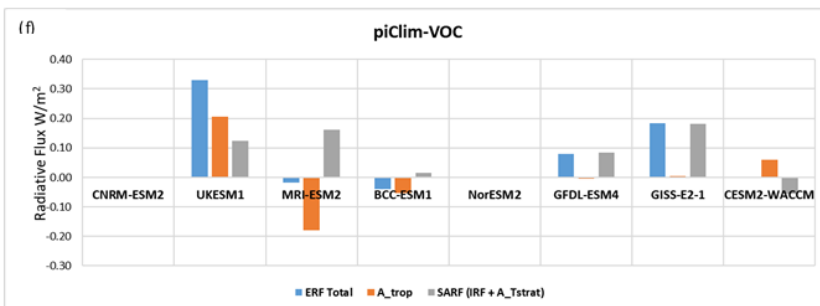
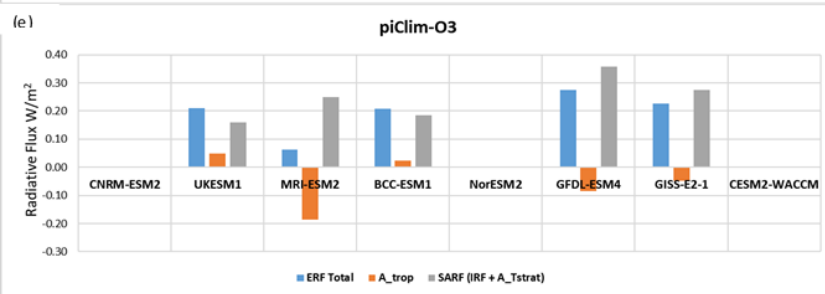
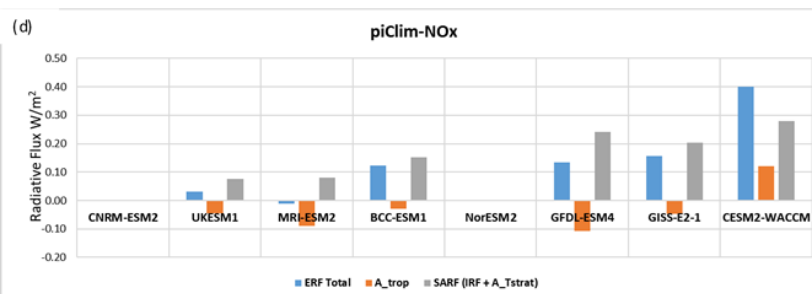
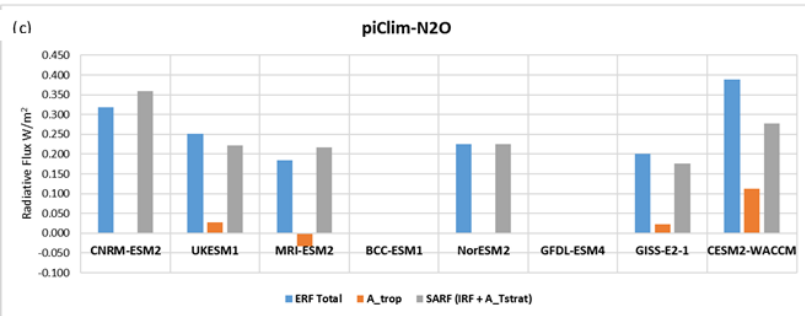
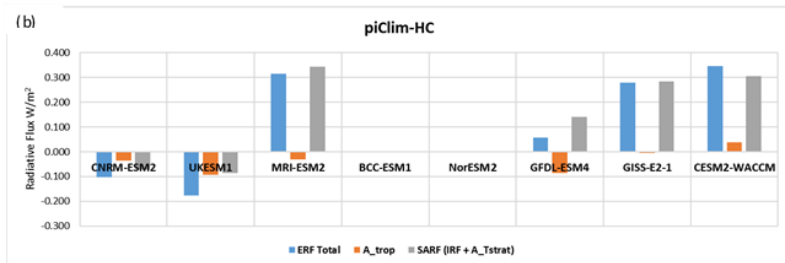
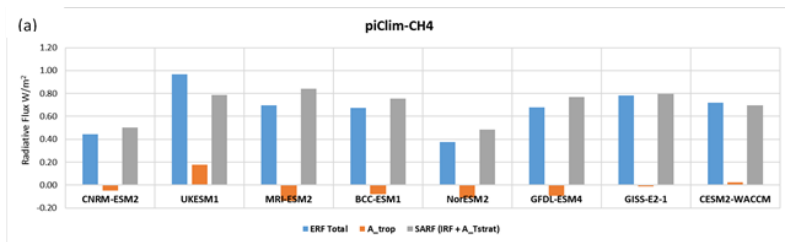


**Figure 6 Breakdown of the ERF into SARF ( $IRF + A_{t, strat}$ ) and tropospheric rapid adjustments ( $A_{trop}$ ) for the chemically reactive species (a) for piClim-CH<sub>4</sub> experiments, (b) for piClim-HC experiments, (c) for piClim-N<sub>2</sub>O experiments, (d) for piClim-NO<sub>x</sub> experiments, (e) for piClim-O<sub>3</sub> experiments, and (f) for piClim-VOC experiments**

503

504

505 **Table 5 Calculations of IRFari, ERFaci (cloud) and ERFcs,af for the chemically reactive species**

	UKESM			GFDL-ESM4			CNRM-ESM2			NorESM2			MRI-ESM2		
	IRFari	ERFcs,af	cloud	IRFari	ERFcs,af	cloud	IRFari	ERFcs,af	cloud	IRFari	ERFcs,af	cloud	IRFari	ERFcs,af	cloud
CH <sub>4</sub>	-0.01	0.86	0.12	-0.01	0.91	-0.22	0.00	0.56	-0.12	-0.01	0.48	-0.10	0.00	0.91	-0.21
HC	-0.02	0.02	-0.18	-0.02	0.22	-0.14	-0.01	-0.02	-0.08				-0.02	0.50	-0.17
N <sub>2</sub> O	-0.01	0.26	0.01				0.00	0.41	-0.09	-0.01	0.24	-0.00	-0.00	0.23	-0.03
O <sub>3</sub>	-0.02	0.16	0.07	-0.04	0.49	-0.18							-0.00	0.24	-0.18
NO <sub>x</sub>	-0.03	0.10	-0.05	-0.02	0.25	-0.09							-0.01	0.03	-0.04
VOC	0.00	0.13	0.20	-0.02	0.18	-0.08							0.004	0.17	-0.2

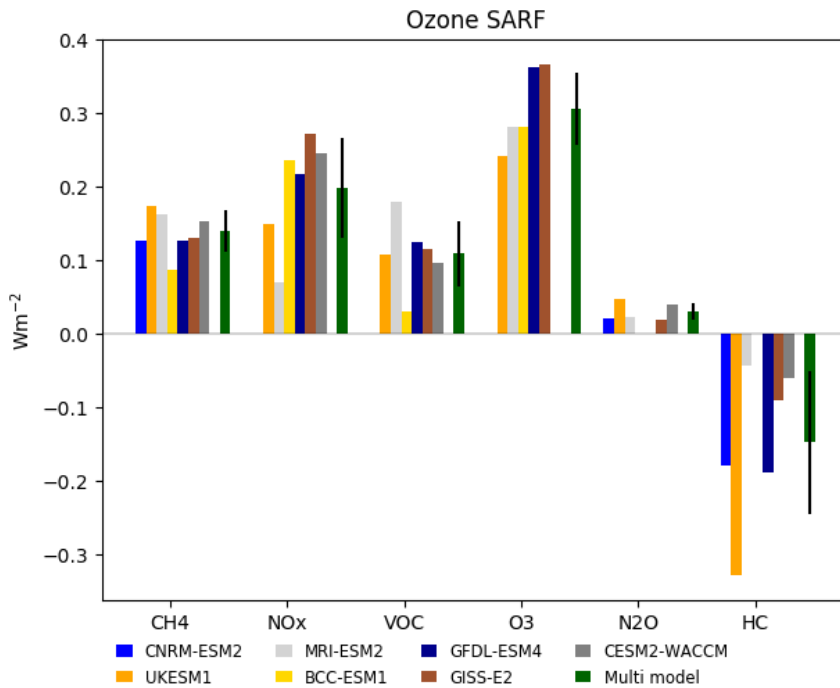
506

507 **4.2.2 Ozone changes**

508 The ozone radiative forcing is diagnosed using a kernel to scale the 3D ozone changes based on Skeie et al. (2020).  
509 This kernel includes stratospheric temperature adjustment, but not tropospheric adjustments so gives a SARF.  
510 These are shown in Fig. 7. Corresponding changes in the tropospheric and stratospheric ozone columns are shown  
511 in figure S5, Increased CH<sub>4</sub> concentrations give a SARF for ozone produced by methane of  $0.14 \pm 0.03 \text{ W m}^{-2}$ ,  
512 anthropogenic NO<sub>x</sub> emissions and VOC (including CO) emissions give SARFs of  $0.20 \pm 0.07$  and  $0.11 \pm 0.04 \text{ W m}^{-2}$   
513 respectively. The O<sub>3</sub> experiment comprised both NO<sub>x</sub> and VOC emission changes. The SARF in this experiment  
514 ( $0.31 \pm 0.05 \text{ W m}^{-2}$ ) is close to the sum of the NO<sub>x</sub> and VOC experiments ( $0.30 \pm 0.05 \text{ W m}^{-2}$  for the same set of  
515 models) showing little non-linearity in the chemistry (Stevenson et al., 2013).

516 There is a larger variation across models in the stratospheric ozone depletion from halocarbons ( $-0.15 \pm 0.10 \text{ W m}^{-2}$ )  
517 with UKESM1 having noticeably larger depletion as seen in Keeble et al. (2020) giving a SARF of  $-0.33 \text{ W m}^{-2}$ .  
518 N<sub>2</sub>O causes some stratospheric ozone depletion in these models, mainly in the tropical upper stratosphere where  
519 depletion causes a positive forcing (Skeie et al., 2020), and increases tropospheric ozone (Fig. S6) giving a small  
520 net positive SARF ( $0.03 \pm 0.01 \text{ W m}^{-2}$ ).

521



522

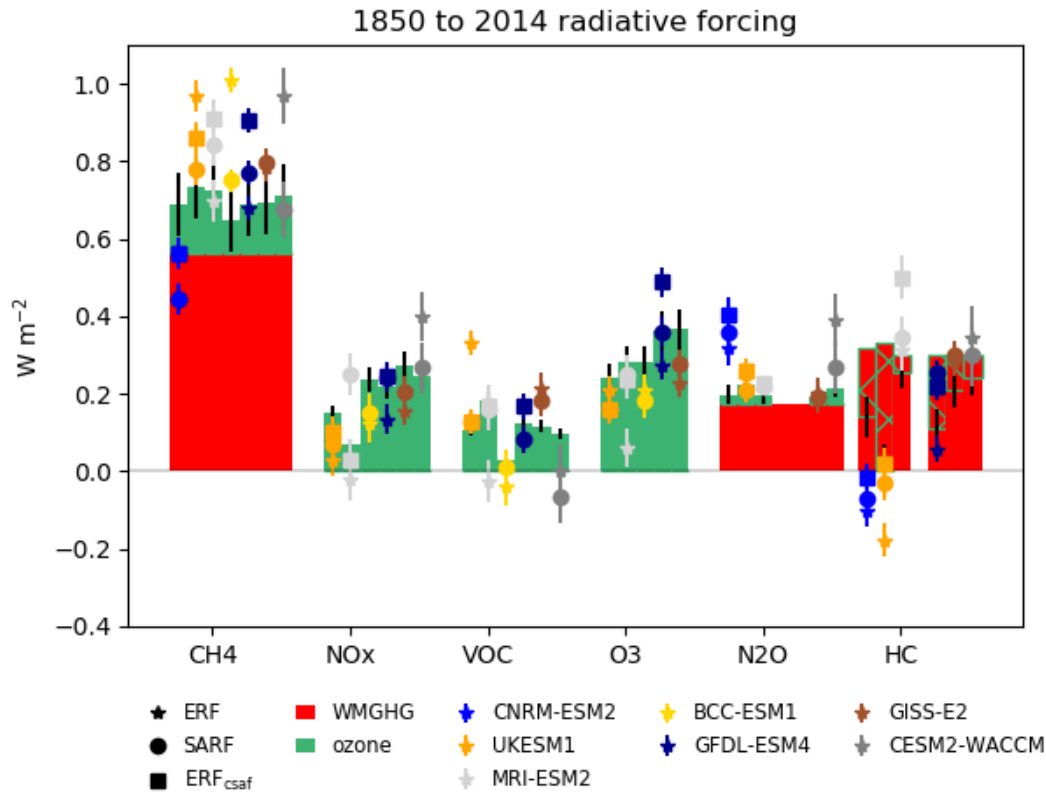
523 **Fig. 7 Changes in ozone stratospheric-temperature adjusted radiative forcing (SARF) for each experiment, diagnosed**  
 524 **using kernels (see text). . Uncertainties for the multi model means are standard deviations across models.**

525 **Methane oxidation also leads to water vapour production. Figure S6 shows increases in the stratosphere for the piClim-**  
 526 **CH4 of up to 20% . The kernel analysis however finds very low radiative forcing associated with this increase**  
 527 **(-0.002±0.003 Wm<sup>-2</sup>).**

#### 528 4.2.3 Comparison with greenhouse gas forcings

529 The ERFs, ERFcs,af and SARFs diagnosed for the greenhouse gas changes (Fig. 6, Table 5) are compared with  
 530 the expected greenhouse gas SARFs in Fig. 8. The expected SARFs from the well-mixed gases are given by  
 531 Etminan et al. (2016) for CH<sub>4</sub> and N<sub>2</sub>O, and by WMO (2018) for the halocarbons (the halocarbon changes are  
 532 slightly different in each model). The expected SARFs from ozone changes are from Fig. 7.

533 For methane the ERFs are typically higher than the expected GHG SARF (except for CNRM-ESM2).The  
 534 diagnosed ERFcs,af and SARF agree better with the expected SARF in UKESM1, BCC-ESM1 and CESM2-  
 535 WACCM, but not in other models. For N<sub>2</sub>O the modelled ERF is larger than the expected SARF for CNRM-  
 536 ESM2-1 and CESM2-WACCM, this is explained by the rapid adjustments for CESM2-WACCM, but not for  
 537 CNRM-ESM2. For halocarbons the stratospheric ozone depletion offsets the direct SARF and accounts for much  
 538 of the spread in the model SARF, although the CNRM-ESM2-1 ERF and SARF is lower than expected. The  
 539 modelled HC ERF for UKESM1 is strongly negative due to increased aerosol cloud interactions, (O'Connor et  
 540 al., 2020a;Morgenstern et al., 2020) but removing cloud effects using the SARF or ERFcs,af agrees better with  
 541 the expected value. The estimated ozone SARF from the NO<sub>x</sub>, VOC and O<sub>3</sub> experiments generally agrees with  
 542 the model SARF and ERFcs,af. For CESM2-WACCM the ERF from the VOC experiment is zero, and the SARF  
 543 negative even though the diagnosed ozone SARF is positive. For all experiments and models ERFcs,af is generally  
 544 higher than the expected or diagnosed SARF (see section 3.3).



545

546 **Fig. 8** Estimated SARF from the greenhouse gas changes (WMGHGs and ozone), using radiative efficiencies for the  
 547 WMGHGs and kernel calculations for ozone (see text). Hatched bars show decreases in ozone SARF. Symbols show  
 548 the modelled ERF, SARF and ERFcsaf (estimate of greenhouse gas clear-sky ERF). Uncertainties on the bars are due  
 549 to uncertainties in radiative efficiencies. Uncertainties on the symbols are errors in the mean due to interannual  
 550 variability in the model diagnostic.

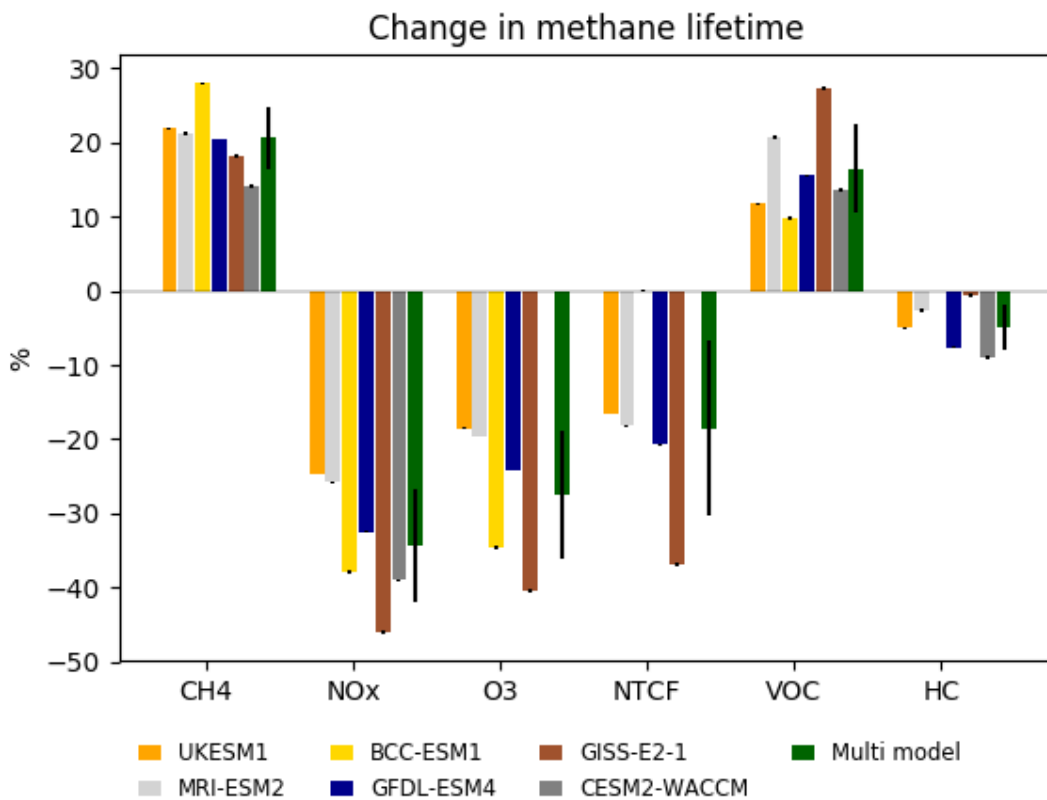
#### 551 4.2.4 Methane Lifetime

552 In the CMIP6 setup the modelled methane concentrations do not respond to changes in oxidation rates. The  
 553 methane lifetime is diagnosed (which includes stratospheric loss to OH as parameterised within each model) and  
 554 assuming losses to chlorine oxidation and soil uptake of 11 and 30 Tg yr<sup>-1</sup> ((Saunois et al., 2020; Myhre et al.,  
 555 2013b) and this can be used to infer the methane changes that would be expected if methane were allowed to vary.  
 556 Fig. 9 shows the methane lifetime response is large and negative for NO<sub>x</sub> emissions, with a smaller positive change  
 557 for VOC emissions. Halocarbon concentration increases decrease the methane lifetime, as ozone depletions leads  
 558 to increased UV in the troposphere and increased methane loss to chlorine in the stratosphere (Stevenson et al.,  
 559 2020). N<sub>2</sub>O also decreases the methane lifetime by depleting ozone in the tropics although the effect is less than  
 560 for halocarbons. The O<sub>3</sub> experiment has a significantly more negative effect (-27±9 %) than the sum of NO<sub>x</sub> and  
 561 VOC (-16±8 %) (uncertainties are multi-model standard deviation). This suggests significant non-additivity. Note  
 562 that a combined CH<sub>4</sub>+NO<sub>x</sub>+VOC experiment is not available to test the additivity further.

563 The lifetime response to changing methane concentrations can be used to diagnose the methane lifetime feedback  
 564 factor *f* ((Fiore et al., 2009). The results here give *f*=1.32, 1.31, 1.43, 1.30, 1.26, 1.19 (mean 1.30±0.07) for  
 565 UKESM1, MRI-ESM2, BCC-ESM1, GFDL-ESM4, GISS-E2-1 and CESM-WACCM. This is in very good  
 566 agreement with AR5, although their values are starting from a year 2000 baseline rather than pre-industrial.

567

568



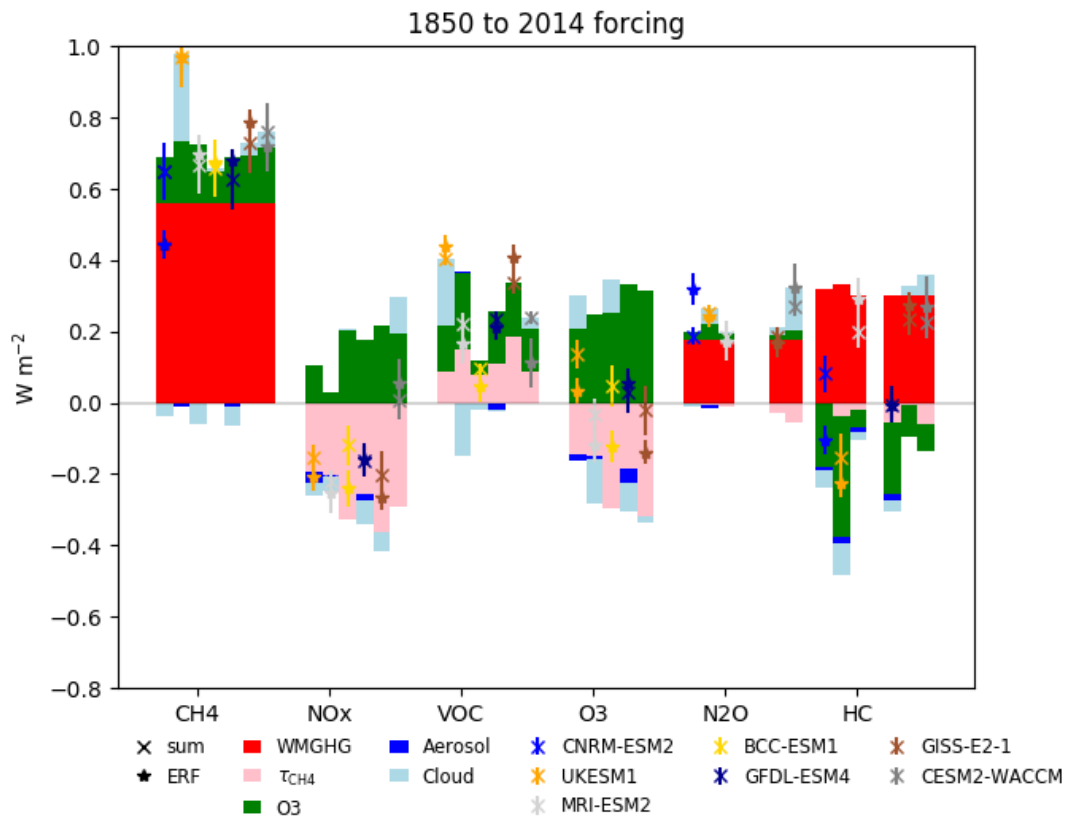
569

570 **Fig. 9** Changes in methane lifetime (%), for each experiment. Uncertainties for individual models are errors on the  
571 mean from interannual variability. Uncertainties for the multi model mean are standard deviations across models.

#### 572 4.2.5 Total ERFs

573 The methane lifetime changes can be converted to expected changes in concentration if methane were allowed to  
574 freely evolve following Fiore et al. (2009), using the *f*-factors appropriate to each model (section 3.3.4). The  
575 inferred radiative forcing is based on radiative efficiency of methane (Etminan et al., 2016). The methane changes  
576 also have implications for ozone production, so we assume an ozone SARF per ppb of CH<sub>4</sub> diagnosed for each  
577 model from section 4.2.

578 The breakdown of the information from the analyses above is shown in Fig. 10, using the SARF calculated for  
579 the gases (WMGHGs and ozone) and kernel-diagnosed cloud adjustments (which include aerosol cloud  
580 interactions). Direct contributions from the aerosols IRFari are shown for models where this is available. The  
581 contributions from methane lifetime changes have also been added to the diagnosed ERF as these aren't accounted  
582 for in the models. Differences between the diagnosed ERF (stars) and the sum of the components (crosses) then  
583 shows to what extent this decomposition into components can account for the modelled ERF. For many of the  
584 species, this breakdown is reasonable, and illustrates that cloud radiative effects can make significant contributions  
585 to the total radiative impacts of WMGHGs and ozone precursors. This analysis cannot distinguish between cloud  
586 effects due to changes in atmospheric temperature profiles or those due to increased cloud nucleation from  
587 aerosols.



588

589 **Fig. 10 SARF for WMGHGs, ozone and diagnosed changes in methane. Model diagnosed direct aerosol RF and cloud**  
 590 **radiative effect. Crosses mark the sum of the five terms for each model. Stars mark the diagnosed ERF with the effect**  
 591 **of methane lifetime (on methane and ozone) added. Differences between stars and crosses shows undiagnosed**  
 592 **contributions. Uncertainties on the sum are mainly due to the uncertainties in the radiative efficiencies. Uncertainties**  
 593 **in the ERF are errors on the mean due to interannual variability. Note for CESM2-WACCM, BCC-ESM1, GISS-E2-1**  
 594 **the direct aerosol effect is unavailable.**

## 595 5. Discussion

596 For all of the species shown we see considerable variation in the calculated ERFs across the models, which is due  
 597 in part to differences in the model aerosol and chemistry schemes; not all models have interactive schemes for all  
 598 of the species, and whether or not chemistry is considered will impact the evolution of some of the aerosol species.  
 599 We can use the differences in model complexity from the multi-model approach together with the separation of  
 600 the effects of the various species in the individual AerChemMIP experiments to understand how the various  
 601 components contribute to the overall ERFs we have calculated.

602

### 603 5.1 Aerosols

604 The 1850-2014 multi-model mean and standard deviation of the ERFs for SO<sub>2</sub>, OC and BC are: -1.03 +/- 0.37  
 605 Wm<sup>-2</sup> for SO<sub>2</sub>, -0.25 +/- 0.09 Wm<sup>-2</sup> for OC, and 0.15 +/- 0.17 Wm<sup>-2</sup> for BC. The total ERF for the aerosols is -  
 606 1.01 +/- 0.25 Wm<sup>-2</sup>, within the range of -1.65 to -0.6 Wm<sup>-2</sup> reported by (Bellouin et al., 2019).

607 The radiative kernels and double-call diagnostics are used to separate the direct and cloud effects of aerosols for  
 608 those models where all the relevant diagnostics are available. These two methods broadly agree on the cloud



609 contribution for the BC, SO<sub>2</sub> and OC experiments. We generally find a weaker total adjustment to black carbon  
610 compared to other studies (Samset and Myhre, 2015;Stjern et al., 2017;Smith et al., 2018). The exceptions are  
611 MIROC6 and GISS-E2-1. These previous studies used much larger changes in black carbon (up to 10 times)  
612 which may cause non-linear effects such as self-lofting.

613 As the ISCCP cloud diagnostics become available for more of the CMIP6 models, it will be possible to do a direct  
614 calculation of the cloud rapid adjustments using the kernels from (Zelinka et al., 2014) and compare those with  
615 the adjustments calculated using the kernel difference method described in (Smith et al., 2018) and used here  
616 (Section 3.2; see also figure 4 and figure S2 from Smith et al. (2020a)).

617 The radiative efficiencies per AOD calculated here are generally larger than those from the AeroCom Phase II  
618 experiments (Myhre et al., 2013b), with the caveat that the models included here did not have fixed clouds, so  
619 that indirect effects would be included.

620 The values diagnosed for the IRFari (for the models we have available diagnostics for) in CMIP6 are similar to  
621 those from CMIP5 (Myhre et al., 2013a) where they reported values for sulfate of -0.4 (-0.6 to -0.2) Wm<sup>-2</sup>  
622 compared to our -0.36 (-0.19 to -0.49) Wm<sup>-2</sup> for the SO<sub>2</sub> experiment, for OC they found -0.09 (-0.16 to -0.03)  
623 Wm<sup>-2</sup> compared to our value of -0.09 (-0.07 to -0.15) Wm<sup>-2</sup> and for BC they had +0.4 (+0.05 to +0.80) compared  
624 to our value of 0.28 (0.13- 0.37) Wm<sup>-2</sup>, so broadly the IRFari for the individual species agree with those found in  
625 the previous set of models used in CMIP5.

626 The overall aerosol ERF from AR5 is reported as in the range -1.5 to 0.4 Wm<sup>-2</sup>, compared to ERF values reported  
627 here for the piClim-aer experiment in the range -0.7 to -1.47 Wm<sup>-2</sup>.

628

## 629 **5.2 Reactive greenhouse gases**

630 The diagnosed ERFs from methane, N<sub>2</sub>O, halocarbons and ozone precursors are: 0.75±0.10, 0.26±0.07, 0.12±0.21  
631 and 0.20±0.07 W m<sup>-2</sup> (excluding CNRM-ESM2-1 for methane as it cannot represent the lower tropospheric ozone  
632 changes, and excluding NorESM2 for all as it has no ozone chemistry). These compare with 0.79±0.13, 0.17±0.03,  
633 0.18±0.15 and 0.22±0.14 W m<sup>-2</sup> for 1750-2011 from AR5 (Myhre et al., 2013a) - where the effects on methane  
634 lifetime and CO<sub>2</sub> have been removed from the AR5 calculations, and the halocarbons are for CFCs and HCFCs  
635 only. Section 4.2.5 shows that cloud effects can make a significant contribution to the overall ERF even for  
636 WMGHGs. However, clouds cannot explain all the differences. The ERF for N<sub>2</sub>O is larger than estimated in AR5.  
637 The ozone contribution here is estimated as 0.03±0.01 Wm<sup>-2</sup> whereas it was zero in AR5, but that does not explain  
638 all the difference. The multi-model ERF for halocarbons is smaller than AR5, due to larger ozone depletion  
639 although the models have a wide spread with some showing significantly lower ERFs and some significantly  
640 higher due to varying strengths of ozone depletion in these models.

641 The estimated ozone SARFs from the changes in levels of methane, NO<sub>x</sub> and VOC from 1850 to 2014 are  
642 0.14±0.03, 0.20±0.07, and 0.11±0.04 W m<sup>-2</sup> compared to 0.24±0.13, 0.14±0.09, and 0.11±0.05 W m<sup>-2</sup> in CMIP5  
643 (Myhre et al., 2013a). The ozone from methane contribution is smaller, here only 25% of the direct Etminan et al.  
644 (2016) methane SARF compared to 50% in AR5 (or 39% using the Etminan et al. (2016) formula). The NO<sub>x</sub>  
645 contribution is larger in this study. The CMIP5 results were based on (Stevenson et al., 2013) in which species  
646 were reduced from present day levels rather than being increased from pre-industrial levels. The NO<sub>x</sub> emission

647 changes are also larger for CMIP6 compared to CMIP5 (Hoesly et al. 2018). The sum of the ozone terms  
648 ( $\text{CH}_4+\text{N}_2\text{O}+\text{HC}+\text{O}_3$ ) is  $0.33\pm 0.11 \text{ Wm}^{-2}$ , agreeing well with the total 1850-2014 ozone SARF of  $0.35 \pm 0.16 \text{ Wm}^{-2}$   
649 (1.s.d) from Skeie et al. (2020) which included a few additional models.

650

651 The overall effect of NTCF emissions (excluding methane and other WMGHGs) on the 1850-2014 ERF  
652 experienced by models that include tropospheric chemistry is strongly negative ( $-0.89\pm 0.20 \text{ W m}^{-2}$ ) due to the  
653 dominance of the aerosol forcing over that from ozone. There is a large spread in the NTCF forcing due to the  
654 different treatment of atmospheric chemistry within these models. Models without tropospheric and/or  
655 stratospheric chemistry prescribe varying ozone levels which are not included in the NTCF experiment. Hence  
656 the overall forcing experienced by these models due to ozone and aerosols will be different from that diagnosed  
657 here.

## 658 **6. Conclusion**

659 The experimental setup and diagnostics in CMIP6 have allowed us for the first time to calculate the effective  
660 radiative forcing (ERF) for present day reactive gas and aerosol concentrations and emissions in a range of Earth  
661 system models. Quantifying the forcing in these models is an essential step to understanding their climate  
662 responses.

663 This analysis also allows us to quantify the radiative responses to perturbations in individual species or groups of  
664 species. These responses include physical adjustments to the imposed forcing as well as chemical adjustments and  
665 adjustments related to the emissions of natural aerosols. The total adjustment is therefore a complex combination  
666 of individual process, but the diagnosed ERF implicitly includes these and represents the overall forcing  
667 experienced by the models.

668 We find that the ERF from well-mixed greenhouse gases (methane, nitrous oxide and halocarbons) has significant  
669 contributions through their effects on ozone, aerosols and clouds, that vary strongly across Earth system models.  
670 This indicates that Earth system processes need to be taken into account when understanding the contribution  
671 WMGHGs have made to present climate and when projecting the climate effects of different WMGHG scenarios.

## 672 **7. Acknowledgements**

673 GT, WC, MM, FMO'C, DO, and MS acknowledge funding received from the European Union's Horizon 2020  
674 research and innovation programme under grant agreement No 641816 (CRESCENDO).

675 D.O. and M.S. were also supported by the Research Council of Norway (grant no. 270061) and by the  
676 Norwegian infrastructure for computational science (grant nos. NN9560K and NS9560K).

677 FMO'C and JPM were funded by the Met Office Hadley Centre Climate Programme funded by BEIS and Defra  
678 (GA01101).

679 CS was supported by a NERC-IIASA Collaborative Research Fellowship (no. NE/T009381/1). GZ was  
680 supported by the NZ government's Strategic Science Investment Fund (SSIF) through the NIWA programme  
681 CACV. MD and NO were supported by the Japan Society for the Promotion of Science (grant numbers:  
682 JP18H03363, JP18H05292, and JP20K04070), the Environment Research and Technology Development Fund

683 (JPMEERF20172003, JPMEERF20202003, and JPMEERF20205001) of the Environmental Restoration and  
684 Conservation Agency of Japan, the Arctic Challenge for Sustainability II (ArCS II), Program Grant Number  
685 JPMXD1420318865, and a grant for the Global Environmental Research Coordination System from the  
686 Ministry of the Environment, Japan. T. T. was supported by the supercomputer system of the National Institute  
687 for Environmental Studies, Japan, and JSPS KAKENHI Grant Number JP19H05669.

688 R.B.S. and G.M. were funded through the Norwegian Research Council project KEYCLIM (grant number  
689 295046) and the European Union's Horizon 2020 Research and Innovation Programme under Grant Agreement  
690 820829 (CONSTRAIN).

691 The CESM project is supported primarily by the National Science Foundation. This material is based upon work  
692 supported by the National Center for Atmospheric Research, which is a major facility sponsored by the NSF  
693 under Cooperative Agreement No. 1852977. Computing and data storage resources, including the Cheyenne  
694 supercomputer (doi:10.5065/D6RX99HX), were provided by the Computational and Information Systems  
695 Laboratory (CISL) at NCAR.

696 We acknowledge the World Climate Research Programme, which, through its Working Group on Coupled  
697 Modelling, coordinated and promoted CMIP6. We thank the climate modeling groups for producing and making  
698 available their model output, the Earth System Grid Federation (ESGF) for archiving the data and providing  
699 access, and the multiple funding agencies who support CMIP6 and ESGF.

700

## 701 **8. Author Contributions**

702 Manuscript preparation was done by GDT, WJC, RJK, DO and additional contributions from all co-authors.  
703 Model simulations were set up, reviewed and/or ran by RChG, DO, FMO'C, NLA, MD, LE, LH, J-FL, MMichou,  
704 MMills, JM, PN, VN, NO, MS, TT, ST, TW, GZ, JZ. Analysis was carried out by GT, WC, RK, DO, RS.

705

## 706 **9. Competing Interests**

707 The authors declare that they have no conflict of interest.

## 708 **10. Data Availability**

709 All data from the various earth system models used in this paper are available on the Earth System Grid Federation  
710 Website, and can be downloaded from there. <https://esgf-index1.ceda.ac.uk/search/cmip6-ceda/>

## 711 **11. References**

712 Ackerman, A. S., Toon, O. B., Taylor, J. P., Johnson, D. W., Hobbs, P. V., and Ferek, R. J.: Effects of  
713 Aerosols on Cloud Albedo: Evaluation of Twomey's Parameterization of Cloud Susceptibility Using  
714 Measurements of Ship Tracks, *Journal of the Atmospheric Sciences*, 57, 2684-2695, 10.1175/1520-  
715 0469(2000)057<2684:eoaoa>2.0.co;2, 2000.

716 Albrecht, B. A.: Aerosols, cloud microphysics, and fractional cloudiness, *Science*, 245, 1227-1230,  
717 1989.

718 Archibald, A. T., O'Connor, F. M., Abraham, N. L., Archer-Nicholls, S., Chipperfield, M. P., Dalvi,  
719 M., Folberth, G. A., Dennison, F., Dhomse, S. S., Griffiths, P. T., Hardacre, C., Hewitt, A. J., Hill, R.,  
720 Johnson, C. E., Keeble, J., Köhler, M. O., Morgenstern, O., Mulchay, J. P., Ordóñez, C., Pope, R. J.,  
721 Rumbold, S., Russo, M. R., Savage, N., Sellar, A., Stringer, M., Turnock, S., Wild, O., and Zeng, G.:  
722 Description and evaluation of the UKCA stratosphere-troposphere chemistry scheme (StratTrop vn 1.0)  
723 implemented in UKESM1, *Geosci. Model Dev. Discuss.*, 2019, 1-82, 10.5194/gmd-2019-246, 2020.

724 Bauer, S. E., Tsigaridis, K., Faluvegi, G., Kelley, M., Lo, K. K., Miller, R. L., Nazarenko, L., Schmidt,  
725 G. A., and Wu, J.: Historical (1850–2014) Aerosol Evolution and Role on Climate Forcing Using the  
726 GISS ModelE2.1 Contribution to CMIP6, *Journal of Advances in Modeling Earth Systems*, 12,  
727 e2019MS001978, 10.1029/2019ms001978, 2020.

728 Bellouin, N., Quaas, J., Gryspeerdt, E., Kinne, S., Stier, P., Watson-Parris, D., Boucher, O., Carslaw,  
729 K. S., Christensen, M., Daniou, A.-L., Dufresne, J.-L., Feingold, G., Fiedler, S., Forster, P., Gettelman,  
730 A., Haywood, J. M., Lohmann, U., Malavelle, F., Mauritsen, T., McCoy, D. T., Myhre, G.,  
731 Müllmenstädt, J., Neubauer, D., Possner, A., Rugenstein, M., Sato, Y., Schulz, M., Schwartz, S. E.,  
732 Sourdeval, O., Storelvmo, T., Toll, V., Winker, D., and Stevens, B.: Bounding global aerosol radiative  
733 forcing of climate change, *Reviews of Geophysics*, n/a, 10.1029/2019rg000660, 2019.

734 Block, K., and Mauritsen, T.: Forcing and feedback in the MPI-ESM-LR coupled model under abruptly  
735 quadrupled CO<sub>2</sub>, *Journal of Advances in Modeling Earth Systems*, 5, 676-691, 10.1002/jame.20041,  
736 2013.

737 Boucher, O. e. a.: Clouds and Aerosols, In: *Climate Change 2013: The Physical Science Basis.*  
738 *Contribution of Working Group I to the Fifth Assessment Report of the Intergovernmental Panel on*  
739 *Climate Change*, in, Cambridge University Press, Cambridge, United Kingdom and New York, NY,  
740 USA., 2013.

741 Checa-Garcia, R., Hegglin, M. I., Kinnison, D., Plummer, D. A., and Shine, K. P.: Historical  
742 Tropospheric and Stratospheric Ozone Radiative Forcing Using the CMIP6 Database, *Geophysical*  
743 *Research Letters*, 45, 3264-3273, 10.1002/2017gl076770, 2018.

744 Chung, E.-S., and Soden, B. J.: An Assessment of Direct Radiative Forcing, Radiative Adjustments,  
745 and Radiative Feedbacks in Coupled Ocean–Atmosphere Models, *Journal of Climate*, 28, 4152-4170,  
746 10.1175/jcli-d-14-00436.1, 2015.

747 Collins, W. J., Lamarque, J. F., Schulz, M., Boucher, O., Eyring, V., Hegglin, M. I., Maycock, A.,  
748 Myhre, G., Prather, M., Shindell, D., and Smith, S. J.: AerChemMIP: quantifying the effects of  
749 chemistry and aerosols in CMIP6, *Geosci. Model Dev.*, 10, 585-607, 10.5194/gmd-10-585-2017, 2017.

750 Deushi, M., and Shibata, K.: Development of a Meteorological Research Institute Chemistry-Climate  
751 Model version 2 for the Study of Tropospheric and Stratospheric Chemistry, *Papers in Meteorology*  
752 *and Geophysics*, 62, 1-46, 10.2467/mripapers.62.1, 2011.

753 Di Biagio, C., Formenti, P., Balkanski, Y., Caponi, L., Cazaunau, M., Pangui, E., Journet, E., Nowak,  
754 S., Andreae, M., Kandler, K., Saeed, T., Piketh, S., Seibert, D., Williams, E., and Doussin, J.-F.:  
755 Complex refractive indices and single scattering albedo of global dust aerosols in the shortwave  
756 spectrum and relationship to iron content and size, *Atmospheric Chemistry and Physics Discussions*, 1-  
757 42, 10.5194/acp-2019-145, 2019.

758 Dunne, J. P., Horowitz, L. W., Adcroft, A. J., Ginoux, P., Held, I. M., John, J. G., Krasting, J. P.,  
759 Malyshev, S., Naik, V., Paulot, F., Shevliakova, E., Stock, C. A., Zadeh, N., Balaji, V., Blanton, C.,  
760 Dunne, K. A., Dupuis, C., Durachta, J., Dussin, R., Gauthier, P. P. G., Griffies, S. M., Guo, H., Hallberg,  
761 R. W., Harrison, M., He, J., Hurlin, W., McHugh, C., Menzel, R., Milly, P. C. D., Nikonov, S., Paynter,  
762 D. J., Ploshay, J., Radhakrishnan, A., Rand, K., Reichl, B. G., Robinson, T., Schwarzkopf, D. M.,

763 Sentman, L. T., Underwood, S., Vahlenkamp, H., Winton, M., Wittenberg, A. T., Wyman, B., Zeng,  
764 Y., and Zhao, M.: The GFDL Earth System Model version 4.1 (GFDL-ESM 4.1): Overall coupled  
765 model description and simulation characteristics, *Journal of Advances in Modeling Earth Systems*, n/a,  
766 e2019MS002015, 10.1029/2019ms002015, 2020.

767 Emmons, L. K., Walters, S., Hess, P. G., Lamarque, J. F., Pfister, G. G., Fillmore, D., Granier, C.,  
768 Guenther, A., Kinnison, D., Laepple, T., Orlando, J., Tie, X., Tyndall, G., Wiedinmyer, C., Baughcum,  
769 S. L., and Kloster, S.: Description and evaluation of the Model for Ozone and Related chemical Tracers,  
770 version 4 (MOZART-4), *Geosci. Model Dev.*, 3, 43-67, 10.5194/gmd-3-43-2010, 2010.

771 Etminan, M., Myhre, G., Highwood, E. J., and Shine, K. P.: Radiative forcing of carbon dioxide,  
772 methane, and nitrous oxide: A significant revision of the methane radiative forcing, *Geophysical*  
773 *Research Letters*, 43, 12,614-612,623, 10.1002/2016gl071930, 2016.

774 Eyring, V., Bony, S., Meehl, G. A., Senior, C. A., Stevens, B., Stouffer, R. J., and Taylor, K. E.:  
775 Overview of the Coupled Model Intercomparison Project Phase 6 (CMIP6) experimental design and  
776 organization, *Geosci. Model Dev.*, 9, 1937-1958, 10.5194/gmd-9-1937-2016, 2016.

777 Fiore, A. M., Dentener, F. J., Wild, O., Cuvelier, C., Schultz, M. G., Hess, P., Textor, C., Schulz, M.,  
778 Doherty, R. M., Horowitz, L. W., MacKenzie, I. A., Sanderson, M. G., Shindell, D. T., Stevenson, D.  
779 S., Szopa, S., Van Dingenen, R., Zeng, G., Atherton, C., Bergmann, D., Bey, I., Carmichael, G., Collins,  
780 W. J., Duncan, B. N., Faluvegi, G., Folberth, G., Gauss, M., Gong, S., Hauglustaine, D., Holloway, T.,  
781 Isaksen, I. S. A., Jacob, D. J., Jonson, J. E., Kaminski, J. W., Keating, T. J., Lupu, A., Marmer, E.,  
782 Montanaro, V., Park, R. J., Pitari, G., Pringle, K. J., Pyle, J. A., Schroeder, S., Vivanco, M. G., Wind,  
783 P., Wojcik, G., Wu, S., and Zuber, A.: Multimodel estimates of intercontinental source-receptor  
784 relationships for ozone pollution, *Journal of Geophysical Research: Atmospheres*, 114,  
785 10.1029/2008jd010816, 2009.

786 Forster, P. M., Richardson, T., Maycock, A. C., Smith, C. J., Samset, B. H., Myhre, G., Andrews, T.,  
787 Pincus, R., and Schulz, M.: Recommendations for diagnosing effective radiative forcing from climate  
788 models for CMIP6, *Journal of Geophysical Research: Atmospheres*, 121, 12,460-412,475,  
789 doi:10.1002/2016JD025320, 2016.

790 Gettelman, A., Mills, M. J., Kinnison, D. E., Garcia, R. R., Smith, A. K., Marsh, D. R., Tilmes, S., Vitt,  
791 F., Bardeen, C. G., McNerny, J., Liu, H. L., Solomon, S. C., Polvani, L. M., Emmons, L. K., Lamarque,  
792 J. F., Richter, J. H., Glanville, A. S., Bacmeister, J. T., Phillips, A. S., Neale, R. B., Simpson, I. R.,  
793 DuVivier, A. K., Hodzic, A., and Randel, W. J.: The Whole Atmosphere Community Climate Model  
794 Version 6 (WACCM6), *Journal of Geophysical Research: Atmospheres*, n/a, 10.1029/2019JD030943,  
795 2019.

796 Ghan, S. J.: Technical Note: Estimating aerosol effects on cloud radiative forcing, *Atmos. Chem. Phys.*,  
797 13, 9971-9974, 10.5194/acp-13-9971-2013, 2013.

798 Hansen, J., Sato, M., Ruedy, R., Nazarenko, L., Lacis, A., Schmidt, G. A., Russell, G., Aleinov, I.,  
799 Bauer, M., Bauer, S., Bell, N., Cairns, B., Canuto, V., Chandler, M., Cheng, Y., Del Genio, A., Faluvegi,  
800 G., Fleming, E., Friend, A., Hall, T., Jackman, C., Kelley, M., Kiang, N., Koch, D., Lean, J., Lerner, J.,  
801 Lo, K., Menon, S., Miller, R., Minnis, P., Novakov, T., Oinas, V., Perlwitz, J., Perlwitz, J., Rind, D.,  
802 Romanou, A., Shindell, D., Stone, P., Sun, S., Tausnev, N., Thresher, D., Wielicki, B., Wong, T., Yao,  
803 M., and Zhang, S.: Efficacy of climate forcings, *Journal of Geophysical Research: Atmospheres*, 110,  
804 10.1029/2005jd005776, 2005.

805 Hoesly, R. M., Smith, S. J., Feng, L., Klimont, Z., Janssens-Maenhout, G., Pitkanen, T., Seibert, J. J.,  
806 Vu, L., Andres, R. J., Bolt, R. M., Bond, T. C., Dawidowski, L., Kholod, N., Kurokawa, J.-i., Li, M.,  
807 Liu, L., Lu, Z., Moura, M. C. P., O'Rourke, P. R., and Zhang, Q.: Historical (1750–2014) anthropogenic

808 emissions of reactive gases and aerosols from the Community Emissions Data System (CEDS),  
809 Geoscientific Model Development (Online), Medium: ED; Size: p. 369-408, 2018.

810 Horowitz, L. W., Naik, V., Paulot, F., Ginoux, P. A., Dunne, J. P., Mao, J., Schnell, J., Chen, X., He,  
811 J., John, J. G., Lin, M., Lin, P., Malyshev, S., Paynter, D., Shevliakova, E., and Zhao, M.: The GFDL  
812 Global Atmospheric Chemistry-Climate Model AM4.1: Model Description and Simulation  
813 Characteristics, *Journal of Advances in Modeling Earth Systems*, n/a, e2019MS002032,  
814 10.1029/2019ms002032, 2020.

815 Johnson, B. T., Haywood, J. M., and Hawcroft, M. K.: Are Changes in Atmospheric Circulation  
816 Important for Black Carbon Aerosol Impacts on Clouds, Precipitation, and Radiation?, *Journal of*  
817 *Geophysical Research: Atmospheres*, 124, 7930-7950, 10.1029/2019jd030568, 2019.

818 Kawai, H., Yukimoto, S., Koshiro, T., Oshima, N., Tanaka, T., Yoshimura, H., and Nagasawa, R.:  
819 Significant improvement of cloud representation in the global climate model MRI-ESM2, *Geosci.*  
820 *Model Dev.*, 12, 2875-2897, 10.5194/gmd-12-2875-2019, 2019.

821 Keeble, J., Hassler, B., Banerjee, A., Checa-Garcia, R., Chiodo, G., Davis, S., Eyring, V., Griffiths, P.  
822 T., Morgenstern, O., Nowack, P., Zeng, G., Zhang, J., Bodeker, G., Cugnet, D., Danabasoglu, G.,  
823 Deushi, M., Horowitz, L. W., Li, L., Michou, M., Mills, M. J., Nabat, P., Park, S., and Wu, T.:  
824 Evaluating stratospheric ozone and water vapor changes in CMIP6 models from 1850-2100, *Atmos.*  
825 *Chem. Phys. Discuss.*, 2020, 1-68, 10.5194/acp-2019-1202, 2020.

826 Lurton, T., Balkanski, Y., Bastrikov, V., Bekki, S., Bopp, L., Braconnot, P., Brockmann, P., Cadule, P.,  
827 Contoux, C., Cozic, A., Cugnet, D., Dufresne, J.-L., Éthé, C., Foujols, M.-A., Ghattas, J., Hauglustaine,  
828 D., Hu, R.-M., Kageyama, M., Khodri, M., Lebas, N., Levvasseur, G., Marchand, M., Ottlé, C., Peylin,  
829 P., Sima, A., Szopa, S., Thiéblemont, R., Vuichard, N., and Boucher, O.: Implementation of the CMIP6  
830 Forcing Data in the IPSL-CM6A-LR Model, *Journal of Advances in Modeling Earth Systems*, 12,  
831 e2019MS001940, 10.1029/2019ms001940, 2020.

832 Matthes, K., Funke, B., Andersson, M. E., Barnard, L., Beer, J., Charbonneau, P., Clilverd, M. A.,  
833 Dudok de Wit, T., Haberreiter, M., Hendry, A., Jackman, C. H., Kretzschmar, M., Kruschke, T., Kunze,  
834 M., Langematz, U., Marsh, D. R., Maycock, A. C., Misió, S., Rodger, C. J., Scaife, A. A., Seppälä, A.,  
835 Shangguan, M., Sinnhuber, M., Tourpali, K., Usoskin, I., van de Kamp, M., Verronen, P. T., and  
836 Versick, S.: Solar forcing for CMIP6 (v3.2), *Geosci. Model Dev.*, 10, 2247-2302, 10.5194/gmd-10-  
837 2247-2017, 2017.

838 Meinshausen, M., Vogel, E., Nauels, A., Lorbacher, K., Meinshausen, N., Etheridge, D. M., Fraser, P.  
839 J., Montzka, S. A., Rayner, P. J., Trudinger, C. M., Krummel, P. B., Beyerle, U., Canadell, J. G., Daniel,  
840 J. S., Enting, I. G., Law, R. M., Lunder, C. R., O'Doherty, S., Prinn, R. G., Reimann, S., Rubino, M.,  
841 Velders, G. J. M., Vollmer, M. K., Wang, R. H. J., and Weiss, R.: Historical greenhouse gas  
842 concentrations for climate modelling (CMIP6), *Geosci. Model Dev.*, 10, 2057-2116, 10.5194/gmd-10-  
843 2057-2017, 2017.

844 Michou, M., Nabat, P., Saint-Martin, D., Bock, J., Decharme, B., Mallet, M., Roehrig, R., Séférian, R.,  
845 Sénési, S., and Voldoire, A.: Present-Day and Historical Aerosol and Ozone Characteristics in CNRM  
846 CMIP6 Simulations, *Journal of Advances in Modeling Earth Systems*, 12, e2019MS001816,  
847 10.1029/2019ms001816, 2020.

848 Morgenstern, O., Braesicke, P., O'Connor, F. M., Bushell, A. C., Johnson, C. E., Osprey, S. M., and  
849 Pyle, J. A.: Evaluation of the new UKCA climate-composition model – Part 1: The stratosphere, *Geosci.*  
850 *Model Dev.*, 2, 43-57, 10.5194/gmd-2-43-2009, 2009.

851 Morgenstern, O., O'Connor, F. M., Johnson, B. T., Zeng, G., Mulcahy, J. P., Williams, J., Teixeira, J.,  
852 Michou, M., Nabat, P., Horowitz, L. W., Naik, V., Sentman, L. T., Deushi, M., Bauer, S. E., Tsigaridis,

853 K., Shindell, D. T., and Kinnison, D. E.: Reappraisal of the climate impacts of ozone-depleting  
854 substances., *Gephys. Res. Lett.*, 2020.

855 Mulcahy, J. P., Johnson, C., Jones, C. G., Povey, A. C., Scott, C. E., Sellar, A., Turnock, S. T.,  
856 Woodhouse, M. T., Abraham, N. L., Andrews, M. B., Bellouin, N., Browse, J., Carslaw, K. S., Dalvi,  
857 M., Folberth, G. A., Glover, M., Grosvenor, D., Hardacre, C., Hill, R., Johnson, B., Jones, A., Kipling,  
858 Z., Mann, G., Mollard, J., O'Connor, F. M., Palmieri, J., Reddington, C., Rumbold, S. T., Richardson,  
859 M., Schutgens, N. A. J., Stier, P., Stringer, M., Tang, Y., Walton, J., Woodward, S., and Yool, A.:  
860 Description and evaluation of aerosol in UKESM1 and HadGEM3-GC3.1 CMIP6 historical  
861 simulations, *Geosci. Model Dev. Discuss.*, 2020, 1-59, 10.5194/gmd-2019-357, 2020.

862 Myhre, G., D. Shindell, F.-M. Bréon, W. Collins, J. Fuglestedt, J. Huang, D. Koch, J.-F. Lamarque,  
863 D. Lee, B. Mendoza, T. Nakajima, A. Robock, G. Stephens, Takemura, T., and Zhang, H.:  
864 Anthropogenic and Natural Radiative Forcing. In: *Climate Change 2013: The Physical Science Basis.*  
865 Contribution of Working Group I to the Fifth Assessment Report of the Intergovernmental Panel on  
866 Climate Change, 2013a.

867 Myhre, G., Samset, B. H., Schulz, M., Balkanski, Y., Bauer, S., Bernsten, T. K., Bian, H., Bellouin, N.,  
868 Chin, M., Diehl, T., Easter, R. C., Feichter, J., Ghan, S. J., Hauglustaine, D., Iversen, T., Kinne, S.,  
869 Kirkevåg, A., Lamarque, J. F., Lin, G., Liu, X., Lund, M. T., Luo, G., Ma, X., van Noije, T., Penner, J.  
870 E., Rasch, P. J., Ruiz, A., Seland, Ø., Skeie, R. B., Stier, P., Takemura, T., Tsigaridis, K., Wang, P.,  
871 Wang, Z., Xu, L., Yu, H., Yu, F., Yoon, J. H., Zhang, K., Zhang, H., and Zhou, C.: Radiative forcing  
872 of the direct aerosol effect from AeroCom Phase II simulations, *Atmos. Chem. Phys.*, 13, 1853-1877,  
873 10.5194/acp-13-1853-2013, 2013b.

874 O'Connor, F. M., Johnson, C. E., Morgenstern, O., Abraham, N. L., Braesicke, P., Dalvi, M., Folberth,  
875 G. A., Sanderson, M. G., Telford, P. J., Voulgarakis, A., Young, P. J., Zeng, G., Collins, W. J., and  
876 Pyle, J. A.: Evaluation of the new UKCA climate-composition model – Part 2: The Troposphere,  
877 *Geosci. Model Dev.*, 7, 41-91, 10.5194/gmd-7-41-2014, 2014.

878 O'Connor, F. M., Abraham, N. L., Dalvi, M., Folberth, G., Griffiths, P., Hardacre, C., Johnson, B. T.,  
879 Kahana, R., Keeble, J., Kim, B., Morgenstern, O., Mulcahy, J. P., Richardson, M. G., Robertson, E.,  
880 Seo, J., Shim, S., Teixeira, J. C., Turnock, S., Williams, J., Wiltshire, A., and Zeng, G.: Assessment of  
881 pre-industrial to present-day anthropogenic climate forcing in UKESM1, *Atmos. Chem. Phys. Discuss.*,  
882 2020, 1-49, 10.5194/acp-2019-1152, 2020.

883 O'Connor, F. M., Abraham, N. L., Dalvi, M., Folberth, G., Griffiths, P., Hardacre, C., Johnson, B. T.,  
884 Kahana, R., Keeble, J., Kim, B., Morgenstern, O., Mulcahy, J. P., Richardson, M. G., Robertson, E.,  
885 Seo, J., Shim, S., Teixeira, J. C., Turnock, S., Williams, J., Wiltshire, A., and Zeng, G.: Assessment of  
886 pre-industrial to present-day anthropogenic climate forcing in UKESM1, *Atmospheric Chemistry and*  
887 *Physics*, Submitted, 2020a.

888 O'Connor, F. M., Jamil, O., Andrews, T., Johnson, B. T., Mulcahy, J. P., and Manners, J.:  
889 Apportionment of the Pre-Industrial to Present-Day Climate Forcing by Methane using UKESM1,  
890 JAMES, submitted, 2020b.

891 Oshima, N., Yukimoto, S., Deushi, M., Koshiro, T., Kawai, H., Tanaka, T. Y., and Yoshida, K.: Global  
892 and Arctic effective radiative forcing of anthropogenic gases and aerosols in MRI-ESM2.0, *Prog. Earth.*  
893 *Planet. Sci.*, 7, 38, <https://doi.org/10.1186/s40645-020-00348-w>, 2020.

894 Pendergrass, A. G., Conley, A., and Vitt, F. M.: Surface and top-of-atmosphere radiative feedback  
895 kernels for CESM-CAM5, *Earth Syst. Sci. Data*, 10, 317-324, 10.5194/essd-10-317-2018, 2018.

896 Pincus, R., and Baker, M. B.: Effect of precipitation on the albedo susceptibility of clouds in the marine  
897 boundary layer, *Nature*, 372, 250-252, 10.1038/372250a0, 1994.

- 898 Pincus, R., Forster, P. M., and Stevens, B.: The Radiative Forcing Model Intercomparison Project  
 899 (RFMIP): experimental protocol for CMIP6, *Geosci. Model Dev.*, 9, 3447-3460, 10.5194/gmd-9-3447-  
 900 2016, 2016.
- 901 Samset, B. H., and Myhre, G.: Climate response to externally mixed black carbon as a function of  
 902 altitude, *Journal of Geophysical Research: Atmospheres*, 120, 2913-2927, 10.1002/2014jd022849,  
 903 2015.
- 904 Samset, B. H., Myhre, G., Forster, P. M., Hodnebrog, Ø., Andrews, T., Faluvegi, G., Fläschner, D.,  
 905 Kasoar, M., Kharin, V., Kirkevåg, A., Lamarque, J.-F., Olivie, D., Richardson, T., Shindell, D., Shine,  
 906 K. P., Takemura, T., and Voulgarakis, A.: Fast and slow precipitation responses to individual climate  
 907 forcings: A PDRMIP multimodel study, *Geophysical Research Letters*, 43, 2782-2791,  
 908 10.1002/2016gl068064, 2016.
- 909 Saunio, M., Stavert, A. R., Poulter, B., Bousquet, P., Canadell, J. G., Jackson, R. B., Raymond, P. A.,  
 910 Dlugokencky, E. J., Houweling, S., Patra, P. K., Ciais, P., Arora, V. K., Bastviken, D., Bergamaschi,  
 911 P., Blake, D. R., Brailsford, G., Bruhwiler, L., Carlson, K. M., Carrol, M., Castaldi, S., Chandra, N.,  
 912 Crevoisier, C., Crill, P. M., Covey, K., Curry, C. L., Etiope, G., Frankenberg, C., Gedney, N., Hegglin,  
 913 M. I., Höglund-Isaksson, L., Hugelius, G., Ishizawa, M., Ito, A., Janssens-Maenhout, G., Jensen, K. M.,  
 914 Joos, F., Kleinen, T., Krummel, P. B., Langenfelds, R. L., Laruelle, G. G., Liu, L., Machida, T.,  
 915 Maksyutov, S., McDonald, K. C., McNorton, J., Miller, P. A., Melton, J. R., Morino, I., Müller, J.,  
 916 Murguía-Flores, F., Naik, V., Niwa, Y., Noce, S., O'Doherty, S., Parker, R. J., Peng, C., Peng, S., Peters,  
 917 G. P., Prigent, C., Prinn, R., Ramonet, M., Regnier, P., Riley, W. J., Rosentretter, J. A., Segers, A.,  
 918 Simpson, I. J., Shi, H., Smith, S. J., Steele, L. P., Thornton, B. F., Tian, H., Tohjima, Y., Tubiello, F.  
 919 N., Tsuruta, A., Viovy, N., Voulgarakis, A., Weber, T. S., van Weele, M., van der Werf, G. R., Weiss,  
 920 R. F., Worthy, D., Wunch, D., Yin, Y., Yoshida, Y., Zhang, W., Zhang, Z., Zhao, Y., Zheng, B., Zhu,  
 921 Q., Zhu, Q., and Zhuang, Q.: The Global Methane Budget 2000–2017, *Earth Syst. Sci. Data*, 12, 1561-  
 922 1623, 10.5194/essd-12-1561-2020, 2020.
- 923 Séférian, R., Nabat, P., Michou, M., Saint-Martin, D., Voltaire, A., Colin, J., Decharme, B., Delire, C.,  
 924 Berthet, S., Chevallier, M., Sénési, S., Franchisteguy, L., Vial, J., Mallet, M., Joetzjer, E., Geoffroy, O.,  
 925 Guérémy, J.-F., Moine, M.-P., Msadek, R., Ribes, A., Rocher, M., Roehrig, R., Salas-y-Méla, D.,  
 926 Sanchez, E., Terray, L., Valcke, S., Waldman, R., Aumont, O., Bopp, L., Deshayes, J., Éthé, C., and  
 927 Madec, G.: Evaluation of CNRM Earth-System model, CNRM-ESM 2-1: role of Earth system  
 928 processes in present-day and future climate, *Journal of Advances in Modeling Earth Systems*, n/a,  
 929 10.1029/2019ms001791, 2019.
- 930 Seland, Ø., Bentsen, M., Seland Graff, L., Olivie, D., Toniazzo, T., Gjermundsen, A., Debernard, J. B.,  
 931 Gupta, A. K., He, Y., Kirkevåg, A., Schwinger, J., Tjiputra, J., Schancke Aas, K., Bethke, I., Fan, Y.,  
 932 Griesfeller, J., Grini, A., Guo, C., Ilicak, M., Hafsahl Karset, I. H., Landgren, O., Liakka, J., Onsum  
 933 Moseid, K., Nummelin, A., Spensberger, C., Tang, H., Zhang, Z., Heinze, C., Iverson, T., and Schulz,  
 934 M.: The Norwegian Earth System Model, NorESM2 - Evaluation of theCMIP6 DECK and historical  
 935 simulations, *Geosci. Model Dev. Discuss.*, 2020, 1-68, 10.5194/gmd-2019-378, 2020.
- 936 Sellar, A. A., Jones, C. G., Mulcahy, J., Tang, Y., Yool, A., Wiltshire, A., O'Connor, F. M., Stringer,  
 937 M., Hill, R., Palmieri, J., Woodward, S., de Mora, L., Kuhlbrodt, T., Rumbold, S., Kelley, D. I., Ellis,  
 938 R., Johnson, C. E., Walton, J., Abraham, N. L., Andrews, M. B., Andrews, T., Archibald, A. T., Berthou,  
 939 S., Burke, E., Blockley, E., Carslaw, K., Dalvi, M., Edwards, J., Folberth, G. A., Gedney, N., Griffiths,  
 940 P. T., Harper, A. B., Hendry, M. A., Hewitt, A. J., Johnson, B., Jones, A., Jones, C. D., Keeble, J.,  
 941 Liddicoat, S., Morgenstern, O., Parker, R. J., Predoi, V., Robertson, E., Siahann, A., Smith, R. S.,  
 942 Swaminathan, R., Woodhouse, M. T., Zeng, G., and Zerroukat, M.: UKESM1: Description and  
 943 evaluation of the UK Earth System Model, *Journal of Advances in Modeling Earth Systems*, n/a,  
 944 10.1029/2019ms001739, 2020.



945 Sherwood, S. C., Bony, S., Boucher, O., Bretherton, C., Forster, P. M., Gregory, J. M., and Stevens, B.:  
946 Adjustments in the Forcing-Feedback Framework for Understanding Climate Change, *Bulletin of the*  
947 *American Meteorological Society*, 96, 217-228, 10.1175/bams-d-13-00167.1, 2015.

948 Shine, K. P., Cook, J., Highwood, E. J., and Joshi, M. M.: An alternative to radiative forcing for  
949 estimating the relative importance of climate change mechanisms, *Geophysical Research Letters*, 30,  
950 10.1029/2003gl018141, 2003.

951 Skeie, R. B., Myhre, G., Hodnebrog, Ø., Cameron-Smith, P. J., Deushi, M., Hegglin, M. I., Horowitz,  
952 L. W., Kramer, R. J., Michou, M., Mills, M. J., Olivie, D. J. L., O'Connor, F. M., Paynter, D., Samset,  
953 B. H., Sellar, A., Shindell, D., Takemura, T., Tilmes, S., and Wu, T.: Historical total ozone radiative  
954 forcing derived from CMIP6 simulations, *npj Climate and Atmospheric Science* 2020.

955 Smith, C. J., Kramer, R. J., Myhre, G., Forster, P. M., Soden, B. J., Andrews, T., Boucher, O., Faluvegi,  
956 G., Fläschner, D., Hodnebrog, Ø., Kasoar, M., Kharin, V., Kirkevåg, A., Lamarque, J.-F., Mülmenstädt,  
957 J., Olivie, D., Richardson, T., Samset, B. H., Shindell, D., Stier, P., Takemura, T., Voulgarakis, A., and  
958 Watson-Parris, D.: Understanding Rapid Adjustments to Diverse Forcing Agents, *Geophysical*  
959 *Research Letters*, 45, 12,023-012,031, doi:10.1029/2018GL079826, 2018.

960 Smith, C. J., Kramer, R. J., Myhre, G., Alterskjær, K., Collins, W., Sima, A., Boucher, O., Dufresne, J.  
961 L., Nabat, P., Michou, M., Yukimoto, S., Cole, J., Paynter, D., Shiogama, H., O'Connor, F. M.,  
962 Robertson, E., Wiltshire, A., Andrews, T., Hannay, C., Miller, R., Nazarenko, L., Kirkevåg, A., Olivie,  
963 D., Fiedler, S., Pincus, R., and Forster, P. M.: Effective radiative forcing and adjustments in CMIP6  
964 models, *Atmos. Chem. Phys.*, 20, 9591-9618, 10.5194/acp-20-9591-2020, 2020a.

965 Smith, C. J., Kramer, R. J., and Sima, A.: The HadGEM3-GA7.1 radiative kernel: the importance of a  
966 well-resolved stratosphere, *Earth Syst. Sci. Data Discuss.*, 2020, 1-16, 10.5194/essd-2019-254, 2020b.

967 Soden, B. J., Held, I. M., Colman, R., Shell, K. M., Kiehl, J. T., and Shields, C. A.: Quantifying Climate  
968 Feedbacks Using Radiative Kernels, *Journal of Climate*, 21, 3504-3520, 10.1175/2007jcli2110.1, 2008.

969 Stevenson, D. S., Young, P. J., Naik, V., Lamarque, J. F., Shindell, D. T., Voulgarakis, A., Skeie, R.  
970 B., Dalsoren, S. B., Myhre, G., Berntsen, T. K., Folberth, G. A., Rumbold, S. T., Collins, W. J.,  
971 MacKenzie, I. A., Doherty, R. M., Zeng, G., van Noije, T. P. C., Strunk, A., Bergmann, D., Cameron-  
972 Smith, P., Plummer, D. A., Strode, S. A., Horowitz, L., Lee, Y. H., Szopa, S., Sudo, K., Nagashima, T.,  
973 Josse, B., Cionni, I., Righi, M., Eyring, V., Conley, A., Bowman, K. W., Wild, O., and Archibald, A.:  
974 Tropospheric ozone changes, radiative forcing and attribution to emissions in the Atmospheric  
975 Chemistry and Climate Model Intercomparison Project (ACCMIP), *Atmos. Chem. Phys.*, 13, 3063-  
976 3085, 10.5194/acp-13-3063-2013, 2013.

977 Stevenson, D. S., Zhao, A., Naik, V., O'Connor, F. M., Tilmes, S., Zeng, G., Murray, L. T., Collins, W.  
978 J., Griffiths, P., Shim, S., Horowitz, L. W., Sentman, L., and Emmons, L.: Trends in global tropospheric  
979 hydroxyl radical and methane lifetime since 1850 from AerChemMIP, *Atmos. Chem. Phys. Discuss.*,  
980 2020, 1-25, 10.5194/acp-2019-1219, 2020.

981 Stjern, C. W., Samset, B. H., Myhre, G., Forster, P. M., Hodnebrog, Ø., Andrews, T., Boucher, O.,  
982 Faluvegi, G., Iversen, T., Kasoar, M., Kharin, V., Kirkevåg, A., Lamarque, J.-F., Olivie, D., Richardson,  
983 T., Shawki, D., Shindell, D., Smith, C. J., Takemura, T., and Voulgarakis, A.: Rapid Adjustments Cause  
984 Weak Surface Temperature Response to Increased Black Carbon Concentrations, *Journal of*  
985 *Geophysical Research: Atmospheres*, 122, 11,462-411,481, 10.1002/2017jd027326, 2017.

986 Suzuki, K., and Takemura, T.: Perturbations to Global Energy Budget Due to Absorbing and Scattering  
987 Aerosols, *Journal of Geophysical Research: Atmospheres*, 124, 2194-2209, 10.1029/2018jd029808,  
988 2019.

- 989 Takemura, T., Nozawa, T., Emori, S., Nakajima, T. Y., and Nakajima, T.: Simulation of climate  
990 response to aerosol direct and indirect effects with aerosol transport-radiation model, *Journal of*  
991 *Geophysical Research: Atmospheres*, 110, 10.1029/2004jd005029, 2005.
- 992 Takemura, T., and Suzuki, K.: Weak global warming mitigation by reducing black carbon emissions,  
993 *Scientific Reports*, 9, 4419, 10.1038/s41598-019-41181-6, 2019.
- 994 Takemura, T., et al: Development of a global aerosol climate model SPRINTARS, CGER's  
995 Supercomputer Monograph Report, 24, 2018.
- 996 Tang, T., Shindell, D., Faluvegi, G., Myhre, G., Olivié, D., Voulgarakis, A., Kasoar, M., Andrews, T.,  
997 Boucher, O., Forster, P. M., Hodnebrog, Ø., Iversen, T., Kirkevåg, A., Lamarque, J.-F., Richardson, T.,  
998 Samset, B. H., Stjern, C. W., Takemura, T., and Smith, C.: Comparison of Effective Radiative Forcing  
999 Calculations Using Multiple Methods, Drivers, and Models, *Journal of Geophysical Research:*  
1000 *Atmospheres*, 124, 4382-4394, 10.1029/2018jd030188, 2019.
- 1001 Tatebe, H., Ogura, T., Nitta, T., Komuro, Y., Ogochi, K., Takemura, T., Sudo, K., Sekiguchi, M., Abe,  
1002 M., Saito, F., Chikira, M., Watanabe, S., Mori, M., Hirota, N., Kawatani, Y., Mochizuki, T., Yoshimura,  
1003 K., Takata, K., O'Ishi, R., Yamazaki, D., Suzuki, T., Kurogi, M., Kataoka, T., Watanabe, M., and  
1004 Kimoto, M.: Description and basic evaluation of simulated mean state, internal variability, and climate  
1005 sensitivity in MIROC6, *Geoscientific Model Development*, 12, 2727-2765,  
1006 <http://dx.doi.org/10.5194/gmd-12-2727-2019>, 2019.
- 1007 Thornhill, G., Collins, W., Olivié, D., Archibald, A., Bauer, S., Checa-Garcia, R., Fiedler, S., Folberth,  
1008 G., Gjermundsen, A., Horowitz, L., Lamarque, J. F., Michou, M., Mulcahy, J., Nabat, P., Naik, V.,  
1009 O'Connor, F. M., Paulot, F., Schulz, M., Scott, C. E., Seferian, R., Smith, C., Takemura, T., Tilmes, S.,  
1010 and Weber, J.: Climate-driven chemistry and aerosol feedbacks in CMIP6 Earth system models, *Atmos.*  
1011 *Chem. Phys. Discuss.*, 2020, 1-36, 10.5194/acp-2019-1207, 2020.
- 1012 Tilmes, S., Hodzic, A., Emmons, L. K., Mills, M. J., Gettelman, A., Kinnison, D. E., Park, M.,  
1013 Lamarque, J. F., Vitt, F., Shrivastava, M., Campuzano-Jost, P., Jimenez, J. L., and Liu, X.: Climate  
1014 Forcing and Trends of Organic Aerosols in the Community Earth System Model (CESM2), *Journal of*  
1015 *Advances in Modeling Earth Systems*, n/a, 10.1029/2019MS001827, 2019.
- 1016 Twomey, S.: Pollution and the planetary albedo, *Atmospheric Environment* (1967), 8, 1251-1256,  
1017 [https://doi.org/10.1016/0004-6981\(74\)90004-3](https://doi.org/10.1016/0004-6981(74)90004-3), 1974.
- 1018 van Marle, M. J. E., Kloster, S., Magi, B. I., Marlon, J. R., Daniau, A. L., Field, R. D., Arneth, A.,  
1019 Forrest, M., Hantson, S., Kehrwald, N. M., Knorr, W., Lasslop, G., Li, F., Mangeon, S., Yue, C., Kaiser,  
1020 J. W., and van der Werf, G. R.: Historic global biomass burning emissions for CMIP6 (BB4CMIP)  
1021 based on merging satellite observations with proxies and fire models (1750–2015), *Geosci. Model Dev.*,  
1022 10, 3329-3357, 10.5194/gmd-10-3329-2017, 2017.
- 1023 Vial, J., Dufresne, J.-I., and Bony, S.: On the interpretation of inter-model spread in CMIP5 climate  
1024 sensitivity estimates, *Climate Dynamics*, 41, 3339-3362, [http://dx.doi.org/10.1007/s00382-013-1725-](http://dx.doi.org/10.1007/s00382-013-1725-9)  
1025 [9](http://dx.doi.org/10.1007/s00382-013-1725-9), 2013.
- 1026 Watanabe, M., Suzuki, T., O'ishi, R., Komuro, Y., Watanabe, S., Emori, S., Takemura, T., Chikira, M.,  
1027 Ogura, T., Sekiguchi, M., Takata, K., Yamazaki, D., Yokohata, T., Nozawa, T., Hasumi, H., Tatebe,  
1028 H., and Kimoto, M.: Improved Climate Simulation by MIROC5: Mean States, Variability, and Climate  
1029 Sensitivity, *Journal of Climate*, 23, 6312-6335, 10.1175/2010jcli3679.1, 2010.
- 1030 Woodward, S.: Modeling the atmospheric life cycle and radiative impact of mineral dust in the Hadley  
1031 Centre climate model, *Journal of Geophysical Research: Atmospheres*, 106, 18155-18166,  
1032 10.1029/2000jd900795, 2001.

- 1033 Wu, T., Lu, Y., Fang, Y., Xin, X., Li, L., Li, W., Jie, W., Zhang, J., Liu, Y., Zhang, L., Zhang, F.,  
1034 Zhang, Y., Wu, F., Li, J., Chu, M., Wang, Z., Shi, X., Liu, X., Wei, M., Huang, A., Zhang, Y., and Liu,  
1035 X.: The Beijing Climate Center Climate System Model (BCC-CSM): the main progress from CMIP5  
1036 to CMIP6, *Geosci. Model Dev.*, 12, 1573-1600, 10.5194/gmd-12-1573-2019, 2019.
- 1037 Wu, T., Zhang, F., Zhang, J., Jie, W., Zhang, Y., Wu, F., Li, L., Liu, X., Lu, X., Zhang, L., Wang, J.,  
1038 and Hu, A.: Beijing Climate Center Earth System Model version 1 (BCC-ESM1): Model Description  
1039 and Evaluation, *Geosci. Model Dev.*, 13, 977-1005, 10.5194/gmd-2019-172, 2020.
- 1040 Yukimoto, S., Kawai, H., Koshiro, T., Oshima, N., Yoshida, K., Urakawa, S., Tsujino, H., Deushi, M.,  
1041 Tanaka, T., Hosaka, M., Yabu, S., Yoshimura, H., Shindo, E., Mizuta, R., Obata, A., Adachi, Y., and  
1042 Ishii, M.: The Meteorological Research Institute Earth System Model Version 2.0, MRI-ESM2.0:  
1043 Description and Basic Evaluation of the Physical Component, *J. Meteor. Soc. Japan*, 97, 931-965,  
1044 10.2151/jmsj.2019-051, 2019.
- 1045 Zelinka, M. D., Andrews, T., Forster, P. M., and Taylor, K. E.: Quantifying components of aerosol-  
1046 cloud-radiation interactions in climate models, *Journal of Geophysical Research: Atmospheres*, 119,  
1047 7599-7615, 10.1002/2014jd021710, 2014.
- 1048